Binary Asteroid Population.
2. Anisotropic distribution of orbit poles of small, inner main-belt binaries

P. Pravec [a], P. Scheirich [a], D. Vokrouhlický [b], A. W. Harris [c],
P. Kušnirák [a], K. Hornoch [a], D. P. Pray [d], D. Higgins [e],
A. Galád [a,f], J. Világi [f], Š. Gajdoš [f], L. Kornoš [f], J. Oey [g],
M. Husárik [h], W. R. Cooney [i], J. Gross [i], D. Terrell [i,j],
R. Durkee [k], J. Pollock [ℓ], D. Reichart [m], K. Ivarsen [m],
J. Haislip [m], A. LaCluyze [m], Yu. N. Krugly [n], N. Gaftonyuk [o],
R. D. Stephens [p], R. Dyvig [q], V. Reddy [r], V. Chiorny [n],
O. Vaduvescu [s,t], P. Longa-Peña [s,u], A. Tudorica [v,w],
B. D. Warner [x], G. Masi [y], J. Brinsfield [z], R. Gonçalves [aa],
P. Brown [ab], Z. Krzeminski [ab], O. Gerashchenko [ac],
V. Shevchenko [n], I. Molotov [ad], F. Marchis [ae,af]

[a] *Astronomical Institute, Academy of Sciences of the Czech Republic, Fričova 1, CZ-25165 Ondřejov, Czech Republic*

[b] *Institute of Astronomy, Charles University, Prague, V Holešovičkách 2, CZ-18000 Prague 8, Czech Republic*

[c] *4603 Orange Knoll Avenue, La Cañada, CA 91011, U.S.A.*

[d] *Carbuncle Hill Observatory, W. Brookfield, MA, U.S.A.*

[e] *Hunters Hill Observatory, Ngunnawal, Canberra, Australia*

[f] *Modra Observatory, Department of Astronomy, Physics of the Earth, and Meteorology, FMFI UK, Bratislava SK-84248, Slovakia*

[g] *Leura Observatory, Leura, N.S.W., Australia*

[h] *Astronomical Institute of the Slovak Academy of Sciences, SK-05960 Tatranská Lomnica, Slovakia*

[i] *Sonoita Research Observatory, 77 Paint Trail, Sonoita, AZ 85637, U.S.A.*

[j] *Deptartment of Space Studies, Southwest Research Institute, Boulder, CO 80302, U.S.A.*

[k] *Shed of Science Observatory, 5213 Washburn Ave. S, Minneapolis, MN 55410, U.S.A.*

[ℓ] *Physics and Astronomy Department, Appalachian State University, Boone, NC 28608, U.S.A.*

[m] *Physics and Astronomy Department, University of North Carolina, Chapel Hill,*

NC 27514, U.S.A.

[n]*Institute of Astronomy of Kharkiv National University, Sumska Str. 35, Kharkiv 61022, Ukraine*

[o]*Crimean Astrophysical Observatory, Simeiz Department, Simeiz 98680, Crimea, Ukraine*

[p]*Center for Solar System Studies, 8300 Utica Avenue, Suite 105, Rancho Cucamonga, CA 91730, U.S.A.*

[q]*Badlands Observatory, 12 Ash Street, P.O. Box 37, Quinn, SD 57775, U.S.A.*

[r]*Department of Space Studies, University of North Dakota, Grand Forks, U.S.A.*

[s]*Instituto de Astronomia, Universidad Catolica del Norte, Avenida Angamos 0610, Antofagasta, Chile*

[t]*Isaac Newton Group of Telescopes, La Palma, Apartado de correos 321, E-38700 Santa Cruz de la Palma, Canary Islands, Spain*

[u]*University of Warwick, Department of Physics, Coventry CV4 7AL, U.K.*

[v]*University of Bucharest, Faculty of Physics, Str. Fizicienilor nr. 1, CP Mg – 11, Bucharest-Magurele 76900, Romania*

[w]*Argelander Institute for Astronomy – Bonn University, Auf dem Huegel 71 D-53121, Germany*

[x]*Palmer Divide Observatory, 17995 Bakers Farm Rd., Colorado Springs, CO 80908, U.S.A.*

[y]*Campo Catino Observatory, I-03016 Guarcino, Italy*

[z]*Via Capote Observatory, Thousand Oaks, CA, U.S.A.*

[aa]*Obs. Ast. de Linhaceira, Escola Superior de Tecnologia de Tomar, Instituto Politecnico de Tomar, 2300-313 Tomar, Portugal*

[ab]*Elginfield Observatory, Department of Physics & Astronomy, University of Western Ontario, London, Ontario N6A 3K7, Canada*

[ac]*Andrushivka Astronomical Observatory, Ukraine*

[ad]*Keldysh Institute of Applied Mathematics, Russian Academy of Sciences, Miusskaya sq. 4, Moscow 125047, Russia*

[ae]*Carl Sagan Center at the SETI Institute, 189 Bernado Av., Mountain View, CA 94043, U.S.A.*

[af]*Department of Astronomy, University of California at Berkeley, Berkeley, CA 94720, U.S.A.*

Editorial correspondence to:

Dr. Petr Pravec

Astronomical Institute AS CR

Fričova 1

Ondřejov

CZ-25165

Czech Republic

Phone: 00420-323-620352

Fax: 00420-323-620263

E-mail address: ppravec@asu.cas.cz

Abstract

Our photometric observations of 18 main-belt binary systems in more than one apparition revealed a strikingly high number of 15 having positively re-observed mutual events in the return apparitions. Our simulations of the survey showed that it cannot be due to an observational selection effect and that the data strongly suggest that poles of mutual orbits between components of binary asteroids in the primary size range 3–8 km are not distributed randomly: The null hypothesis of an isotropic distribution of the orbit poles is rejected at a confidence level greater than 99.99%. Binary orbit poles concentrate at high ecliptic latitudes, within 30° of the poles of the ecliptic. We propose that the binary orbit poles oriented preferentially up/down-right are due to either of the two processes: (i) the YORP tilt of spin axes of their parent bodies toward the asymptotic states near obliquities 0 and 180° (pre-formation mechanism), or (ii) the YORP tilt of spin axes of the primary components of already formed binary systems toward the asymptotic states near obliquities 0 and 180° (post-formation mechanism). The alternative process of elimination of binaries with poles closer to the ecliptic by dynamical instability, such as the Kozai effect due to gravitational perturbations from the Sun, does not explain the observed orbit pole concentration. This is because for close binary asteroid systems, the gravitational effects of primary's irregular shape dominate the solar-tide effect.

Key words: Asteroids, binary;

1 Introduction

Orientation of the orbital plane of components in a binary asteroid can be estimated from photometric observations of their mutual events — occultations/eclipses. It requires observations taken over a range of geometries of the system with respect to Earth and Sun. Scheirich and Pravec (2009) derived or constrained orbit poles of 5 near-Earth asteroid binaries, taking advantage of rapid changes of viewing geometries of the near-Earth binaries during their approaches to Earth. Binary systems in the main belt of asteroids show a limited change of observing geometry during one apparition [1] and observations over 2–3 apparitions are typically needed to estimate the orientation (ecliptic longitude and latitude of the pole) of the mutual orbit for a main-belt asteroid (MBA) binary.

We run a photometric survey for binaries among small asteroids since 2005. Among 477 MBAs surveyed until May 2011, we found 45 binaries. Of them, 18 were re-observed in their return apparitions. Using the technique of Pravec et al. (2006) and Scheirich and Pravec (2009), we analysed the data and estimated or constrained mutual orbits of the 18 binaries observed in 2–3 apparitions. An interpretation of the sample of derived binary parameters must take into account existing observational biases, see a theory of the selection effects of the photometric technique of binary detection presented in Sect. 2. A direct estimation of the biases present in the discovered sample of binaries is complicated by a limited probability of covering the mutual event in a binary with *a priori* unknown orbit period with a given set of survey observations. This complication is overcome with analysis of the statistics of re-detections of mutual events in the binaries in their return apparitions. The key advantage is that a time distribution of the planned follow-up observations of the binaries in the return apparitions was matched to their orbit periods determined in the discovery apparition, which made our simulations of the observational selection effects feasible.

2 Probability of photometric detection of a binary asteroid

The probability of the photometric detection of a binary asteroid is formulated as follows:

$$P_{\text{det}} = p_{\text{me}} \, p_{\text{cov}} \, p_{\text{res}} \,, \tag{1}$$

---

[1] An asteroid's photometric apparition is a time interval, usually a few weeks to a few months long, when the asteroid is in favorable conditions (brightness, solar elongation) allowing photometric observations of required accuracy and duration during night. For main belt asteroids, it occurs around opposition with the Sun.

where p_{me} is a probability of occurrence of a mutual event (occultation or eclipse) between the components of the system, p_{cov} is a probability of covering the mutual event with a given set of observations, and p_{res} is a probability of resolving the mutual event with the given photometric observations.

The probability of occurrence of a mutual event depends on the parameters of the system:

$$p_{\mathrm{me}} \equiv p_{\mathrm{me}}(\epsilon, a_{\mathrm{orb}}, e, D_1, D_2, \text{component shapes}, \text{phase effect}) \,, \tag{2}$$

where ϵ is an obliquity of the mutual orbit of the binary components, a_{orb} and e are its semimajor axis and eccentricity, D_i is a mean diameter of the i-th component ($D_2 \leq D_1$), and the probability also depends on shapes of the components and their phase effect. In a general case, the p_{me} function is complex and it can be described with a numerical model. A qualitative understanding can be, however, obtained with analysing the special case of a system with spherical components, zero eccentricity of the mutual orbit, and zero solar phase, for which we get the following analytical formula:

$$p_{\mathrm{me}} = \begin{cases} 1, & \text{if } \epsilon \leq i_{\mathrm{c}} \text{ or } \epsilon \geq (\pi - i_{\mathrm{c}}) \,, \\ \frac{2}{\pi} \arcsin \frac{\sin i_{\mathrm{c}}}{\sin \epsilon} \,, & \text{if } i_{\mathrm{c}} < \epsilon < (\pi - i_{\mathrm{c}}) \,, \end{cases} \tag{3}$$

where

$$i_{\mathrm{c}} = \arcsin \frac{1 + \frac{D_2}{D_1}}{2 \frac{a_{\mathrm{orb}}}{D_1}} \,. \tag{4}$$

Figure 1 shows the p_{me} function for three values of $\sin i_{\mathrm{c}}$, which cover a range of this parameter for the binaries in our studied sample. The abscissa of $|\cos \epsilon|$ was chosen because an isotropic distribution of poles gives an uniform distribution in $\cos \epsilon$. The plot illustrates the existing observational selection effect of the photometric method favoring detections of binaries with obliquities close to 0 and 180°. The probablility of occurrence of mutual events reaches a minimum at obliquity $\epsilon = \frac{\pi}{2}$: $p_{\mathrm{me}}(\epsilon = \frac{\pi}{2}) = \frac{2}{\pi} i_{\mathrm{c}}$, but it increases only slowly with increasing $|\cos \epsilon|$ until ϵ reaches $\sim 30°$ or 150°. This selection effect causes that an observed distribution of $|\cos \epsilon|$ has a median value of ~ 0.7 for an original isotropic distribution of orbit poles (which has the median $|\cos \epsilon|$ of 0.5). In other words, the selection effect modifies the original isotropic distribution with a half of systems having obliquities within $\pm 30°$ of 90° to an observed distribution with a half of observed binaries with obliquities within about $\pm 45°$ of 90°.

The mean probability of occurrence of mutual events is

$$P_{\mathrm{me}} = \frac{\int_0^\pi p_{\mathrm{me}}(\epsilon) f(\epsilon) \, \mathrm{d}\epsilon}{\int_0^\pi f(\epsilon) \, \mathrm{d}\epsilon} \,, \tag{5}$$

6

where $f(\epsilon)$ is a number density of binary orbit poles. In the case of the isotropic distribution of binary orbits, $f(\epsilon) = \sin \epsilon$, we get

$$P_{\mathrm{me}} = 1 - \cos i_{\mathrm{c}} + \int\limits_{i_{\mathrm{c}}}^{\pi/2} p_{\mathrm{me}}(\epsilon) \sin \epsilon \, \mathrm{d}\epsilon \ . \tag{6}$$

After further manipulation, we get

$$P_{\mathrm{me}} = \sin i_{\mathrm{c}} = \frac{1 + \frac{D_2}{D_1}}{2\frac{a_{\mathrm{orb}}}{D_1}} \ . \tag{7}$$

This describes another selection effect of the photometric method favoring detections of close systems; the mean probability of occurrence of mutual events for the isotropic distribution of orbit poles is inversely proportional to the relative distance a_{orb}/D_1 between the components. This selection effect is apparent also from Eq. (3) and Fig. 1, with p_{me} being greater for closer systems with greater i_{c}. We point out that for real observations taken generally at non-zero solar phases, the mutual event occurrence probabilities are increased by a factor between 1 and 2 depending on the actual solar phase.

The probability of covering the mutual event with a given set of observations:

$$p_{\mathrm{cov}} \equiv p_{\mathrm{cov}}(P_{\mathrm{orb}}, \text{time distribution of observations}) \ , \tag{8}$$

where P_{orb} is a mutual orbit period of the binary components. For a given distribution of observations, the probability has to be computed with a numerical model. Nevertheless, a general trend is that this probability decreases with increasing orbit period, further strengthening the selection effect towards close systems. This probability is usually less than 1 for observations of a previously unknown binary where the orbit period is not known *a priori* and thus a distribution of the observations cannot be matched to the orbit period. In a case of planned re-observations of a known binary with determined orbit period, however, the probability can be effectively set to 1 with scheduling the observations so that to cover the full orbit. This highly simplifies simulations of planned observations of known binaries in their return apparitions and allows us to constrain a distribution of their orbit poles with analysis of the re-observations in the post-discovery apparitions.

The probability of resolving mutual event, p_{res}, depends on a depth of the mutual event (F) and photometric quality of the observations. The depth of (relative brightness attenuation in) a total secondary event at zero solar phase is $F_{\mathrm{sec}} = I_2/(I_1 + I_2)$, where I_i is a light flux from the i-th component. For components with the same albedo observed at zero phase angle, it converts to $F_{\mathrm{sec}} = [1 + (D_1/D_2)^2]^{-1}$, and the depth of the primary event is $F_{\mathrm{prim}} = F_{\mathrm{sec}}$. At non-zero phase angles and for non-central events, the depth of the mutual event is computed with a numerical model, assuming a specific scattering law.

The photometric quality of the observations affects the probability of resolving the mutual event substantially. Generally, events with depth much greater than photometric errors of the observations are resolved with a probability approaching 1, while events with depth lower than the photometric errors are usually buried in the noise and the probability of resolving them is close to 0. For observations producing controlled and homogeneous data, the probability of resolving mutual event is approximated with a step function:

$$p_{\text{res}} = \begin{cases} 0, & \text{if } F < F_{\text{lim}} , \\ 1, & \text{if } F \geq F_{\text{lim}} , \end{cases} \tag{9}$$

where F_{lim} is a minimum detectable relative brightness attenuation.

Being equipped with the theory of photometric detection of a binary asteroid, we will interpret our observations of binary asteroids presented in Section 3 with simulations of the survey observations given in Section 4.

3   Observations and binary parameters estimations

We run a long-term project of photometric observations of binary systems among small asteroids called "Photometric Survey for Asynchronous Binary Asteroids" since 2005. The collaborating station Palmer Divide Observatory runs a parallel survey project aimed at describing rotations and binary systems in the Hungaria asteroids group (Warner et al. 2009a,c). Both surveys used similar observing techniques and strategies, and they actually cooperated and coordinated their observations; there was a major overlap of the lists of stations participating in the two surveys. We joined observations of binaries made within the two cooperating surveys and analysed them together as they effectively worked as one joint binary asteroids survey.

Of 45 MBA binaries that we detected within the surveys by May 2011, 18 were re-observed in their return apparitions. The re-observations were done for binaries that returned in favorable observational conditions (brightness allowing getting photometric errors ≤ 0.03 mag, position in the sky allowing observations longer than a few hours and away from dense star fields at low galactic latitudes). No prediction of a probability of occurrence of mutual events in the second apparition based on observations from the first apparition was made, so the selection of binaries for re-observations was not affected by their orbit poles.

Using methods described in Pravec et al. (2006), Pravec and Harris (2007), and Scheirich and Pravec (2009), we estimated or constrained parameters of the 18 binary systems, they are listed in Table 1. The modeling technique and its modifications accounting for precession of the pericenter of an eccentric orbit and for possible presence of a third body in three of the studied systems are

outlined in Section 3.1. The observations as well as additional estimated parameters are given in the electronic Supplementary Information. A comprehensive table with the estimated parameters, including their uncertainties and references, is available at web page http://www.asu.cas.cz/∼asteroid/binastdata.htm. The original photometric data will be stored in ALCDEF archive (Stephens et al. 2010).

Of the 18 binaries observed in more than one apparition, we detected mutual events in 15 also upon their return. In the three cases of negative event detection in the return apparition, there were observed no apparent attenuations with relative depth of 4% or greater. We cannot rule out possible occurrence of very shallow events with depths below the 4%-event depth detection limit of our survey, due to grazing eclipses or occultations; an occurrence of such near-boundary events producing attenuations below the detection limit are accounted for in the model of the survey that we present in the next section.

In Table 2, we list epochs and asteroid's ecliptic longitudes and latitudes with respect to Earth (L, B) and Sun $(L_{\mathrm{h}}, B_{\mathrm{h}})$ of the first observing session with positive event detection in both the discovery and the return apparitions for each of the 18 binaries. These were the key data for the simulations of the binary survey that we present in Section 4. For the three systems that did not show mutual events in the return apparition, we list an epoch of the observing session closest to the middle of the observational run (that lasted from 3 to 17 days in the three cases).

3.1 Binary models

We modeled the binary systems using the technique of Scheirich and Pravec (2009), modified to allow for precession of the pericenter. The observational data were reduced using the standard technique described in Pravec et al. (2006); a rotation lightcurve of the primary was fitted and subtracted from the data. In three cases, namely Pogson, Polonskaya and Litva, there was present also a second rotational lightcurve component with period different from P_{orb}. Its character leads us to suspect that it belongs to a third body in the system, see our reasoning given in the discussions for the three asteroids below. To account for presence of the third body, a total light flux scattered towards observer was computed as $I_1 + I_2 + I_3$, where I_i is the light flux from the i-th body. As we did not constrain I_3 from our observations (as we saw no mutual events involving the third body), we run our models for the three systems with a few values of I_3 in a range from 0 and I_1, i.e., sampling the size range of the suspect third body from negligible size up to a size equal to that of the primary. This way we estimated a sensitivity of our results on the size of the third body.

In our model we represent irregular shape of the binary components with ellipsoids of revolution, namely an oblate spheroid for the primary and a prolate

spheroid for the secondary, orbiting each other on Keplerian orbit. The secondary was assumed to rotate synchronously and its long axis was aligned with the centers of the two bodies. Eccentricities of the mutual orbits were found to be small, from 0 up to an upper limit that reached values from 0.03 (for 1453 Fennia) up to 0.20 for the case of (17260) 2000 JQ58 with the least constrained eccentricity. In modeling the eccentric orbit, a precession of the line of apsides was computed. A pericenter drift rate depends on primary's polar flattening (see Murray and Dermott 1999, eq. 6.249) that was only poorly estimated from our observations —the primary's axial ratio a_1/c_1 was constrained to be in a range from 1 up to a certain upper limit in most cases— and we fitted the pericenter drift rate as an independent parameter. Its initial values were stepped in a range from zero to 30°/day; this range encompasses all possible values for the flattening and other parameters of the modeled binaries. To reduce a complexity of the modeling, the upper limit on eccentricity was estimated by fitting data from the best-covered apparition only. In modeling data from all apparitions together, we set the eccentricity equal zero, neglecting possible small effects of the pericenter precession.

The estimated model parameters are given in Table 1. The resulting pole areas for 9 systems with unique solutions plus (2044) Wirt with a double but narrow solution are shown in Figs. 2 to 20 (figures with even numbers). All uncertainties and admissible ranges of the parameters estimated by the numerical models correspond to 3σ confidence level (see Scheirich and Pravec 2009). Examples of the data for the orbital lightcurve components together with the synthetic lightcurves for the best-fit solutions are presented in Figs. 3 to 21 (figures with odd numbers). The results for most systems are rather routine and they are obvious from the table and figures, but we comment below on the three systems where we suspect the presence of a third body. Overall our estimated poles are at high ecliptic latitudes. We find it also interesting that they are often close to the pole of the osculating heliocentric orbit of the binary (generally precessing in space).

(1830) Pogson

We observed this system in three apparitions: from 2007-04-18.4 to 2007-06-06.6, from 2008-09-02.8 to 2008-11-06.8, and from 2010-02-20.6 to 2010-04-08.7. In all the three apparitions, the lightcurve data revealed two rotational components with superimposed mutual events. The two rotational components have periods of (2.57003±0.00006) h and (3.2626±0.0004) h (the uncertainties are 1σ) with apparent amplitudes of 0.10–0.12 and 0.03 mag, respectively. Both rotational components are present at all orbital phases including mutual events, with unchanged shape in the event. The fact that the second rotational component does not disappear in mutual events indicates that it is not a rotation of the secondary. We consider that it may rather belong to a third body in the system.[2] This proposed explanation will have to be confirmed and

---

[2] An alternative explanation of that the apparent second rotational period could be due to an excited rotation of the primary is not supported as the data do not

a size and distance of the third body will have to be estimated with future observations.

A solution for the pole and period of the mutual orbit given in Table 1 and shown in Fig. 6 was obtained by fitting our model to the data for the orbital lightcurve component, derived with subtracting both rotational components, from all the three apparitions simultaneously. We analysed an effect of possible presence of the third body on our modeling and estimated parameters. The size ratio $D_2/D_1 = 0.30 \pm 0.02$ that was estimated from the depth of the secondary mutual event becomes a lower limit if there is a third body contributing to the total light of the system. Thus, in addition to running our orbit modeling with the size ratio estimate of 0.30 that corresponds to a zero or negligible size of the third body, we run the model also for a few cases with the third body having a diameter in the range from zero up to D_1. We found that the presence of the third body had a negligible effect on the estimated orbit period, but it affected the estimated orbit pole area. The admissible area of the pole shrinks by up to a factor of three with the third body's diameter increasing up to the diameter of the primary (see Fig. 6).

(2006) Polonskaya

We observed this system in three apparitions: from 2005-11-01.0 to 2005-12-07.1, from 2008-06-04.3 to 06.4, and from 2010-01-10.1 to 2010-02-22.3. Mutual events were observed in the first and the third apparition only. In the second apparition, we covered 61% of the orbit and there did not occur mutual events with depth greater than 0.02 mag.

In all the three apparitions, the lightcurve data revealed two rotational components (with superimposed mutual events in the first and the third apparition). The two rotational components have periods of (3.11809 ± 0.00007) h and (6.6593 ± 0.0004) h (the uncertainties are 1σ) with apparent amplitudes of 0.08–0.10 and 0.07–0.10 mag, respectively. Like in the case of (1830) Pogson described above, both rotational components of Polonskaya were present at all orbital phases including mutual events with unchanged shapes in the events, suggesting that it is not a rotation of the secondary but that it may rather belong to a third body in the system. Like for Pogson, this will have to be confirmed with future observations.

Combining data from the first and the last apparitions, we found five solutions for the period and two solutions for the pole of the mutual orbit, fitting our model to the data for the orbital lightcurve component, derived with subtracting both rotational components. The estimated periods are $P_{\mathrm{orb}} = 19.1407$ h, 19.1507 h, 19.1553 h, 19.1607 h and 19.1654 h, with 3-σ errors 0.0001–0.0002 h. Limiting values of the ecliptic latitudes for the admissible areas of the orbit

---

show a significant signal at linear combinations of the two observed frequencies; the two rotational components appear purely additive (cf. data for tumbling asteroids in Pravec et al. 2005).

pole are $B_p > +54°$ and $< -60°$ (for model bulk density > 1.0 g cm^{-3} the values of B_p are constrained to be $> +71°$ and $< -72°$).

An attempt to join in the data from the 2008 apparition where there occurred no event deeper than 0.02 mag failed; for all the solutions from the 2005+2010 data, there were predicted observable events to occur during the times of the 2008 observations. This leads us to consider that some assumption of the model might not hold. In particular, it is possible that the mutual orbit plane of the components was not constant and that it precessed. If so, then the joint solution of the 2005 and 2010 observations may be spurious.

(2577) Litva

We observed this system in two apparitions: from 2009-02-28.1 to 2009-04-01.9, and from 2010-07-16.2 to 2010-08-31.3. In both apparitions, the lightcurve data revealed two rotational components with superimposed mutual events. In the 2010 apparition, the two rotational components had periods of 2.8129 h and 5.6818 h with predominating uncertainties due to the synodic-sidereal effect that were estimated to be about 0.0001 h and 0.0004 h, respectively. In the 2009 apparition when there was a larger synodic-sidereal effect (about 0.0003 h and 0.002 h, respectively), the two periods were 2.8126 h and 5.684 h. Apparent amplitudes of the two rotational components were 0.17 and 0.06 mag at solar phases 11°–22° in 2010, while they were somewhat greater, 0.24 and 0.09 mag at higher solar phases of 22°–30° in the 2009 apparition. Inspecting the behavior of the rotational components in the 2009 data where the mutual events were covered thoroughly, we found both components were present at all orbital phases including mutual events, with apparently unchanged shapes in the events. The fact that the second rotational component does not disappear in mutual events indicates that it is not a rotation of the secondary. Like in the similar cases of (1830) Pogson and (2006) Polonskaya, we consider that the second rotational component may rather belong to a third body in the system.

A solution for the pole and period of the mutual orbit given in Table 1 and shown in Fig. 10 was obtained by fitting our model to the data for the orbital lightcurve component, derived with subtracting both rotational components, from both apparitions simultaneously. We analysed the effect of possible presence of the third body on our modeling and estimated parameters. From the depth of the mutual events observed in 2009, we estimated the size ratio $D_2/D_1 = 0.34 \pm 0.02$. Analogously with the case of (1830) Pogson, in addition to running our orbit modeling with the size ratio estimate of 0.34 that corresponds to a zero or negligible size of the third body, we run the model also for a few cases with the third body having a diameter in the range from zero up to D_1. We found that the presence of the third body had a negligible effect on the estimated orbit period and only a small effect on the estimated orbit pole area; the admissible area of the pole shrinks by $\sim 20\%$ with the third body's diameter increasing up to the diameter of the primary (see Fig. 10).

4 Simulations of the survey

The rate of 15 positive re-detections of the 18 binaries in their return apparitions is strikingly high. We simulated the survey, tested the null hypothesis of isotropic distribution of binary orbit poles and found that it is rejected at a high confidence level. We found that poles of mutual orbits of small binaries concentrate at high ecliptic latitudes around the poles of the ecliptic. We present results of the simulations in this section.

The model of the binary survey is analogous to that we used for simulations of our survey for near-Earth asteroid binaries in Pravec et al. (2006), except that in the present work we allowed for non-isotropic orbit pole distribution. We used the following assumptions and approximations:

- Uniform distribution of orbit poles in L_{p} and in (a) $|\sin B_{\mathrm{p}}| = \sin B_{\mathrm{x}}$ to 1, or (b) $|\cos \epsilon| = \cos \epsilon_{\mathrm{x}}$ to 1, where B_{x} and ϵ_{x} is a lower and upper limit cutoff of the distribution in ecliptic latitude and obliquity, respectively. For $B_{\mathrm{x}} = 0$ and $\epsilon_{\mathrm{x}} = 90°$, it is the isotropic distribution.
- Zero eccentricity of the mutual orbit.
- Spherical shape of both components.
- Same albedos for both components.
- Lommel-Seeliger scattering law for the distribution of apparent surface brightness over the disc (see Kaasalainen et al. 2002).
- Bulk density of 2.0 g/cm^3. The same bulk density is assumed for both components, i.e., the mass ratio is estimated as $(D_2/D_1)^3$.
- The probability of resolving mutual event is approximated with the step function given by Eq. (9): $p_{\mathrm{res}} = 0$ and 1 for the relative brightness attenuation depth $F < 4\%$ and $\geq 4\%$ of total light, respectively.

Except for the assumed distribution of binary orbit poles, which is actually the property that we were testing in this work, the assumptions and approximations given above are supported by the observational data for the binaries, or plausible ranges of deviation from them could not have significant effects in the simulations. Only one of the assumptions, namely that of the bulk density of 2.0 g/cm^3, is not well constrained and it could produce a small but possibly not entirely negligible systematic effect if not held; if the binaries had systematically lower or higher bulk densities than the assumed value, then detection rates resulting from the simulations would be under- or overestimated, respectively. A qualitative analysis of their effect on our simulations suggests that systematically lower bulk densities would not affect our conclusions, and only if the asteroid binaries had systematically much higher bulk densities we would have to analyse their effects to our simulations closely. Such much higher bulk densities appear unlikely, and we stay with the assumed value that is close to the best estimate of a binary asteroid bulk density of 1.97 ± 0.24 g/cm^3 for 1999 KW4 (Ostro et al. 2006).

As given in the first item above, we run the simulations for two variant distributions of binary orbit poles: (a) orbit poles concentrated towards the poles

of the ecliptic, and (b) orbit poles concentrated towards the poles of current osculating heliocentric orbits of binary systems. The case (a) may be more relevant, for following reasons: While being spun up by the YORP effect, the asteroid's pole moves towards the Cassini state 2 or 3, which both shift towards the poles of the ecliptic with the precession constant decreasing with increasing spin frequency (see, e.g., Eq. (17) in Colombo 1966). For non-zero inclination of the heliocentric orbit (i_{h}), the asteroid's pole oscillates around the obliquity equal to i_{h} or $(180° - i_{\mathrm{h}})$, though YORP alone would work towards more extreme obliquity values. See Sect. 5 for details and further discussion.

In each simulation, we randomly generated 30000 orbit poles with a chosen distribution in $|\sin B_{\mathrm{p}}|$ or $|\cos \epsilon|$. For each pole and each of the 18 binaries, we computed whether there occurred mutual events (with relative attenuation depth $\geq 4\%$) for the first, discovery apparition epoch. If there occurred an observable mutual event at the first apparition epoch, which is a requirement for binary detection with our technique, then this case represents a positive detection of the binary in the first apparition.[3] For the positive detection, we then computed whether there occurred an observable event also at the second, return apparition epoch. A resulted rate of occurrence of positive re-detections in the return apparition for each of the 18 binaries was recorded. Results of the simulations for the assumed isotropic distribution of binary orbit poles (the null hypothesis) and for one of the tested anisotropic distributions, namely the uniform distribution in $|\cos \epsilon|$ from $\sin 60°$ to 1, are shown in Table 3. There, n_{1stapp} is a number of positive detections of the binary for the 30000 random orbit pole generations, n_{2ndapp} is a number of positive re-detections of the n_{1stapp} binaries detected in the first apparition, and the probability of a positive re-detection is given in the next column.[4] The median probability of positive re-detection for the 18 binaries is ~ 0.30 for the isotropic distribution.

A correspondence of the results from the numerical model with the analytical theory for the special case presented in Section 2 is illustrated in Fig. 22 where we plot relative frequencies of the initial positive detections (the data in the n_{1stapp} column in Table 3) for the assumed isotropic distribution, cf. with Fig. 1. Note that the numerical model accounts also for non-zero solar phase of the observations as well as for the p_{res} function, these effects modify the p_{me} function.

---

[3] Here we assume that the probability p_{cov} of covering the mutual event with observations in the discovery apparition is independent of the orbit pole orientation. In fact it is not exactly so, as for non-central events, the event duration is shorter than for central ones, thus there may be a slight dependence of p_{cov} on orbit pole position. We neglect this minor effect in our simulations.

[4] For most of the binaries, the computed probability of a positive re-detection in the return apparition was in a range from 0.17 to 0.41 for the assumed isotropic distribution of binary orbit poles. Two of them, (2577) Litva and (5477) Holmes had, however, a higher probability of positive re-detection (0.74 and 0.80). This was because the return apparitions of the two binaries happened to be placed approximately diametrically opposite in their heliocentric orbits with respect to the discovery apparition, resulting in the enhanced probability of re-detection.

14

After completing the simulation with the 30000 random generations for a given test distribution of orbit poles, we then used the resulted probabilities of positive re-detections and computed a probability density of getting $N_{2\mathrm{app}}$ positive re-detections of the 18 studied binaries. The probability density was computed by random generating positive/negative detections for the 18 binaries with the estimated individual probabilities ($n_{2\mathrm{ndapp}}/n_{1\mathrm{stapp}}$), repeated 10000 times. Relative frequencies of getting $N_{2\mathrm{app}}$ positive re-detections of the 18 cases in the 10000 random generations were plotted in a histogram and the resulted probability density of positive re-detections was then compared to the observed number of 15 of the 18 binaries actually showing mutual events in their return apparitions.

The null hypothesis of the isotropic distribution of binary orbit poles ($B_{\mathrm{x}} = 0, \epsilon_{\mathrm{x}} = 90°$) is rejected at a high confidence level. The simulation gave that an expected number of positive re-detections was 6 ± 3 (the 95% probability interval) and a probability of getting 15 positive re-detections among the 18 studied binaries was $< 10^{-4}$ (see Fig. 23).

The high observed number of positive re-detections indicates that there is a lack of binary orbit poles at low ecliptic latitudes (at obliquities around 90°) and that they concentrate at high ecliptic latitudes. To estimate how large is the concentration of orbit poles towards the poles of the ecliptic or, alternatively, towards the poles of current binary heliocentric orbits, we run the simulations for several trial distributions with poles distributed uniformly in the range $|\sin B_{\mathrm{p}}| = \sin B_{\mathrm{x}}$ to 1, and $|\cos \epsilon| = \cos \epsilon_{\mathrm{x}}$ to 1.

For B_{x} as well as $(90° - \epsilon_{\mathrm{x}}) \leq 30°$, a probability of getting ≥ 15 positive re-detections of the 18 binaries remains low, $< 10^{-3}$. The probability becomes noticeable for the cutoff latitude/co-obliquity values greater than $\sim 45°$, see Figs. 24 to 27 where we present the resulted probability density distributions for B_{x} and $(90° - \epsilon_{\mathrm{x}}) = 45°, 53°, 60°$, and 70°. For the test distribution concentrated towards the ecliptic poles, the probability is estimated to be 1%, 4%, and 9% for the distribution cut at $B_{\mathrm{x}} = 53°, 60°$, and 70°, respectively. For the alternative distribution of binary poles concentrated towards the heliocentric orbit poles, the probability is estimated to be 1%, 7%, and $> 15\%$ for the distribution cut at $(90° - \epsilon_{\mathrm{x}}) = 45°, 53°, \geq 60°$, respectively.

The simulations suggest that binary orbit poles concentrate within $\sim 30°$ of the ecliptic poles, or alternatively, within $\sim 40°$ of the heliocentric orbit poles. They do not distinguish which one of the two hypotheses —binary poles concentration in ecliptic latitude vs concentration in obliquity— is valid; a theoretical study of this problem is given in Sect. 5. We point out that the trial pole distributions with a step function at given ecliptic latitude or co-obliquity are arbitrary and that an actual distribution of binary orbit poles may be more gradual. In any case, the conslusions reached above from the re-detection statistics support our estimates/constraints for individual pole orientations in Sect. 3 that indeed concentrate within 30° of the ecliptic poles.

5 Interpretation and Discussion

Binary systems among small asteroids (primary diameters $D_1 \lesssim 10$ km) appear to form from parent bodies spinning at a critical rate by some sort of fission or mass shedding process (Scheeres 2007, Pravec and Harris 2007, Walsh et al. 2008, Jacobson and Scheeres 2011). A mechanism to spin the parent asteroid up to its critical rotation frequency is provided by the Yarkovsky-O'Keefe-Radzievskii-Paddack (YORP) effect (e.g., Bottke et al. 2006). While spinning it up, the YORP effect also changes the asteroid's spin orientation toward a YORP end state (see, e.g., Čapek and Vokrouhlický 2004). Thus, by reaching the critical spin frequency the parent bodies may get an anisotropic distribution of spin orientations with poles concentrating near the YORP asymptotic states. This is supported by analysis of distribution of pole orientation for single asteroids in the main belt with sizes ≤ 30 km, appropriate for parent bodies of our binary systems (e.g., Hanuš et al. 2011). After the formation of a binary, the primary component may experience a further evolution by YORP, again toward a YORP endstate. Additionally, life of a binary asteroid may be troubled by instability due to perturbations from mutual gravitational effects[5] and those from the solar tidal field.

We consider three hypotheses for origin of the anisotropic distribution of binary orbit poles:

(1) The preferentially up/down-right orientation of binary orbit poles is set up upon their formation, i.e., it reflects orientations of spin vectors of their parent bodies with poles evolved toward the YORP asymptotic states near 0° and 180°.
(2) Binaries formed with a broader distribution of orbit poles but later they were YORP-tilted towards the YORP asymptotic states on a long timescale.
(3) Binaries with poles close to the ecliptic plane were eliminated due to instability triggered by some dynamical process(es).

In Section 5.1 below we examine a short-term dynamical evolution of binary asteroids using a simple numerical model, showing that it does not support the hypothesis (3) above. In Section 5.2 we then briefly discuss the hypotheses (1) and (2), but a thorough model of the long-term evolution of the binary systems is left for a future work.

---

[5] This applies for very compact systems. Main-belt binaries analysed in this paper have components distant enough that their mutual gravitational effects should not be able to produce major instability.

5.1 Short-term dynamical evolution of binary systems in our sample

5.1.1 General considerations

At the first sight, the reported situation is reminiscent of irregular satellites of giant planets, whose inclination relative to the ecliptic plane also avoids values around the polar orbit. In that case, the solar-tide perturbation has been found to drive large oscillations of the satellite eccentricity and inclination in the non-populated inclination region, the process generally known as the Kozai dynamics (e.g. Kozai 1962, Carruba et al. 2002, Nesvorný et al. 2003). Eventually, the pericenter distance would have been too small and impacts on regular satellites of the planet would occur.

Here, however, the situation is different and the observed satellites in the binary systems are analogs of the regular, rather than irregular, satellites of giant planets. This is because of their close proximity to the primary. Assuming reasonable flattening of the latter, in quantitative terms $\gamma = c_1/a_1 \leq 0.97$ where c_1 and a_1 are polar and mean equatorial radii of the dynamically equivalent ellipsoid (i.e., ellipsoid with the same moments of inertia) of the primary (see Appendix), the Laplace plane of the satellite motion tilts from the ecliptic to the equatorial plane of the primary for distances smaller than several tens of primary radii[6] (e.g., Goldreich 1965, Mignard 1981). This means that the quadrupole perturbation due to the primary oblateness dominates the solar-tide effect. In particular, it drives fast pericenter circulation which effectively inhibits the Kozai mechanism.[7] As a result the whole binary system acts as a single gyroscope on a heliocentric orbit. The latitude variations of its angular momentum may still be non-trivial, due to interaction with the precession of the heliocentric orbit of the binary, but overall no major dynamical instability at low ecliptic latitudes is expected.

5.1.2 Simple numerical model

In order to verify the picture outlined in the previous paragraphs, we constructed a simple numerical model that tracks orbital evolution of the satellite and the spin of the primary. The assumptions make the model valid only over a short timespan of $\simeq$ My, but it still provides a basic tool to verify binary orbital pole stability at low ecliptic latitudes; note that the Kozai instability timescale is much shorter, several thousands of years only. Formulation and basic features of the model are given in the Appendix. In what follows we provide three different examples of a short-term orbital evolution for binaries

---

[6] The distance from the primary at which solar-tide effects take over the primary oblateness effect can be estimated by $d_2 \simeq [2\,(C-A)\,a_h^3/m_0]^{1/5}$, where A and C are equatorial and polar moments of inertia of the primary, a_h is the semimajor axis of the binary's heliocentric orbit and m_0 the solar mass.

[7] Frozen orbits with $d\omega/dt = 0$ at critical inclination with respect to the primary's equatorial plane (e.g. Breiter and Elipe 2006) are not considered in this paper.

from our observed sample.

Low-inclination, main belt binary: (4029) Bridges. First, we choose the case of (4029) Bridges residing on low-inclination, main belt heliocentric orbit. Because it is located outside the 3/1 mean motion resonance with Jupiter, the proper frequency of nodal precession of its heliocentric orbit is rather large, $s \simeq -51.8$ arcsec/yr, while the proper inclination is only moderate $\simeq 5.9°$. Its contribution is well separated from the forced term at $s_6 \simeq -26.3$ arcsec/yr frequency and only $\simeq 1°$ amplitude in the Fourier spectrum of the non-singular inclination vector $\zeta = q + \imath p = \sin I/2 \exp(\imath \Omega)$ of the heliocentric orbit.

Figure 28 shows a sample of binary orbit pole evolutions for various initial latitudes and longitudes equal to $\Omega + 90°$ (left panel) and $\Omega + 270°$ (right panel); Ω is the longitude of ascending node of the heliocentric orbit. Additionally, the evolution shown by the thick curve on the left panel corresponds to the initial pole position $(L_{\mathrm{p}}, B_{\mathrm{p}}) = (305°, -85°)$ very close to the osculating pole of the heliocentric orbit and near the center of the uncertainty region of the solution (Fig. 16). For any initial latitude value the evolution is very stable, showing only very small oscillations driven by solar torque on the system and small heliocentric orbit inclination with respect to the ecliptic. This is because the effective precession constant of the system, see Eq. (11) below, is $\simeq 20$ arcsec/yr, well separated from both s and s_6 terms in ζ.

High-inclination, Hungaria binary: (1453) Fennia. Next, we consider the case of Hungaria-type binary (1453) Fennia, residing on high-inclination heliocentric orbit. In this case the spectrum of ζ is dominated by the proper term with frequency $s \simeq -20.4$ arcsec/yr and proper inclination of $\simeq 24.4°$, but there are more planetary terms with similar frequencies. Of particular interest may be the $s_4 \simeq -17.8$ arcsec/yr with forced inclination $\simeq 0.4°$ and the $s_6 \simeq -26.3$ arcsec/yr with forced inclination $\simeq 0.2°$.

Figure 29 shows the same numerical experiment as above for (4029) Bridges, notably a short numerical integration of the Fennia system with different initial latitude values of its orbit pole. The thick curve on the left panel shows a possible evolution of the orbit pole for this binary for initial position $(L_{\mathrm{p}}, B_{\mathrm{p}}) = (95°, -66°)$ very close to the osculating pole of the heliocentric orbit and near the center of the uncertainty region of our solution (Table 1 and Fig. 4). Here we see a much different picture, with individual tracks of the orbit pole showing large oscillations, especially for positive latitude value (prograde sense of binary motion). Since these oscillations are significantly larger than the proper inclination value of the heliocentric orbit, the situation warrants a closer analysis.

Our results obviously confirm that: (i) the primary's oblateness efficiently locks the satellite orbit to its equatorial plane, and (ii) the satellite orbit maintains to be quasi-circular (with only very small oscillations of the osculating eccentricity value). Henceforth, the Kozai mechanism is inhibited for any initial value of orbit pole, even if in the ecliptic plane ($B_{\mathrm{p}} = 0°$). Rotation of the primary and revolution of the satellite thus couple together and act as a single

gyroscope with the angular momentum composed of the two contributions. In order to understand the general pattern of its ecliptic-latitude evolution from Fig. 29, one must determine the appropriate precession constant α of the system.

For a single asteroid, let us say the primary in the pair with $\alpha = \alpha_{\mathrm{prim}}$, rotating about the principal axis of the inertia tensor we have

$$\alpha_{\mathrm{prim}} = \frac{3}{2} \frac{n_{\mathrm{h}}^2}{\omega} \frac{C - A}{C} \,, \tag{10}$$

where n_{h} is the mean motion of the heliocentric revolution, ω is the angular rotation frequency, C and A are the principal moments of the inertia tensor about the polar and equatorial axes (e.g., Bertotti et al. 2003). However, the presence of the satellite modifies the situation. The gravitational torque due to the Sun now acts both on the primary and the satellite orbit. The precession constant of the whole binary system α_{eff} thus reads (e.g., Ward 1975, French et al. 1993)

$$\alpha_{\mathrm{eff}} = \frac{3}{2} \frac{n_{\mathrm{h}}^2}{\omega} \frac{J_2 + q}{\lambda + l} \,, \tag{11}$$

where $J_2 = (C - A)/(m_1 R_1^2)$, $\lambda = C/(m_1 R_1^2)$, $q = m_2 a_{\mathrm{orb}}^2/(2 m_1 R_1^2)$ and $l = m_2 a_{\mathrm{orb}}^2 n_{\mathrm{b}}/(m_1 R_1^2 \omega)$ (with m_1 mass of the primary and R_1 its effective radius, m_2 mass of the satellite, a_{orb} semimajor axis of the satellite orbit and n_{b} is the mean motion of the binary components revolution about their center of mass; see Appendix for more details). Here, respectively, q is the effective contribution of the satellite orbit to the dynamical flattening measured by the quadrupole coefficient J_2, and l is the orbital angular momentum of the satellite relative to the rotational angular momentum of the primary. We note that l is typically a small contribution to λ in the denominator of Eq. (11), meaning most of the angular momentum is in the rotation of the primary. On the contrary, unless very large oblateness of the primary, q dominates contribution of J_2 in the numerator of Eq. (11). In conclusion, the precession constant of the binary system is larger than that of solitary primary as a result of the satellite presence. For (1453) Fennia, for instance, we would have $\alpha_{\mathrm{prim}} \simeq 14.9$ arcsec/yr for the primary only (assuming oblateness $\gamma = c_1/a_1 = 0.89$, cf. Appendix), but the true value according to Eq. (11) with data in Table 1 is $\alpha_{\mathrm{eff}} \simeq 85$ arcsec/yr. This is a much larger frequency, which has subtle implications. For instance, the primary's precession constant would imply only two proper-frequency Cassini states [8] at high latitudes. However, the true system with larger α_{eff} value has four proper-frequency Cassini states, with the Cassini state 2 at only $\simeq 36°$ latitude (Fig. 29, left panel). Also the newly bifurcated Cassini state 1 is at $\simeq 58°$ latitude and longitude offset by $270°$ from the longitude of ascending node of Fennia's heliocentric orbit (Fig. 29,

---

[8] Detailed discussion of the Colombo top model and Cassini states can be found in Colombo (1966), Henrard and Murigande (1987) or Vokrouhlický et al. (2006).

right panel). Orbit pole evolution may oscillate about these states with large amplitude. The solutions for initially retrograde poles show a much more regular evolution with the amplitude of latitude oscillations basically given by the inclination of the binary's heliocentric orbit.

High-inclination, main belt binary: (2044) Wirt. Finally, we consider the case of (2044) Wirt, residing on high-inclination orbit with semimajor axis value in the inner part of the main belt. In fact, with its mean perihelion at $\simeq 1.65$ AU only (and osculating value reaching down to $\simeq 1.42$ AU), this asteroid is on an escaping route to the planet crossing zone. The spectrum of ζ is dominated by the proper-frequency term with $s \simeq -43.3$ arcsec/yr and about $\sim 23.5°$ proper inclination amplitude, but it also contains a large number of contributions from the forced planetary frequencies and their linear combinations with s (all having amplitudes of $\simeq 2.2°$ and smaller).

Figure 30 shows again a sample of possible pole evolutions with different initial orientations, including those that start near the middle of our two solutions from Table 1 and Fig. 8 (shown as thick curves). The general behavior of the solutions can again be understood in terms of a modification of precession constant due to the satellite: assuming a polar oblateness $\gamma = c_1/a_1 = 0.75$ of the primary, we would have $\alpha_{\mathrm{prim}} \simeq 13.3$ arcsec/yr that becomes $\alpha_{\mathrm{eff}} \simeq 33.7$ arcsec/yr with the satellite (for smaller oblateness values, larger γ, both α_{prim} and α_{eff} are smaller, but the gross results are not changed unless $\gamma > 0.9$). The α_{eff} value is large enough to significantly displace Cassini state 2, especially since (2044) Wirt has a high inclination of the heliocentric orbit, to $\simeq 46°$ distance from the heliocentric orbit pole. This puts the Cassini state 2 at $\simeq 67°$ ecliptic latitude, right in the zone of our prograde solution for this system (see the thick curve on the left panel of Fig. 30). An exact location at the Cassini state 2 would also require $180°$ longitude difference between the pole of the heliocentric orbit and the binary pole; we find that our prograde solution is only $\sim 40°$ away, implying a small amplitude circulation about the Cassini state 2. Smaller polar oblateness values for the primary would displace the Cassini state 2 to slightly higher ecliptic latitude value and would imply larger amplitude oscillation of the orbit pole of (2044) Wirt. The high-inclination and high-eccentricity state of the Wirt heliocentric orbit, with occasional crossing of the Mars orbit, makes the behavior of ζ only quasi-periodic. Its truncated Fourier representation is only approximate and includes unusual prograde precessing terms which produce long-period variations in the pole latitude of our solutions near $B_{\mathrm{p}} \simeq -50°$.

We conclude that while the examples of Hungaria-type binary, (1453) Fennia, and Phocaea-type binary, (2044) Wirt, above show that latitude of the orbit pole may have non-trivial evolution, they do not provide evidence for larger stability at high latitudes versus low latitudes. On the contrary: if we were to run orbit pole evolutions for denser and initially isotropic distribution, we would obtain a homogeneous occupation of any latitude (in $\cos B_{\mathrm{p}}$ measure) over a time. This experiment has been performed by Vokrouhlický et al. (2006) for single asteroids, but as we proved that the compact binaries effectively be-

have like single objects with only modified precession constant, it applies also here. We thus conclude, that for the observed parameters of the binary systems, their dynamics is stable over a My timescale even for very small ecliptic latitudes of the orbital pole. Assuming an initially isotropic distribution of poles, it should remain an isotropic distribution at any moment of time.

While the pole stability at all latitudes is true population-wise, we return to the issue of possibly complicated latitude tracks of individual objects with very large oscillations in the prograde zone. This especially applies to binaries which have large inclination value of their heliocentric orbit with respect to the ecliptic; notable examples are Hungaria and Phocaea groups (see Vokrouhlický et al. 2006). In these cases, the latitude value of the current orbit pole position of the binary may not directly reflect its initial value. Only a more detailed information about the system, such as a constraint on the polar flattening of the primary, would provide more insight in the possible evolutionary tracks of the pole.

5.2 Long-term dynamical evolution: hints and guesses

Our numerical model provides an information about the observed binary systems over a timescale which might be only a snapshot in their lifetime. While, the observed (tidal) synchronization of the satellite's rotation implies ages longer than $\sim (1-10)$ My (e.g., Taylor and Margot 2010, 2011), we have only a loose handle of the upper age limit. The collisional lifetime of the km-size satellites suggests that most of the binary systems in our sample are not older than $\sim (200-500)$ My (e.g., Bottke et al. 2005) and a similar, or longer, timescale is obtained by non-synchronization of the rotation rate of the primary. This is a long time, over which weak torques like the YORP effect might act on the systems. For instance, distribution of the spin orientations of single asteroids is skewed toward the ecliptic poles in a good agreement with a steady-state model with the YORP effect (e.g., Hanuš et al. 2011). In the same way, YORP acting on the primary component should slowly tilt the system toward the asymptotic YORP states, presumably at large ecliptic latitudes.

Using data in Čapek and Vokrouhlický (2004) we find that near-critically rotating $\simeq 8$ km asteroid in the inner part of the main belt should tilt its pole position by $\simeq 10°$ per 100 My on average. Because of the $\propto 1/D^2$ scaling of the YORP strength, a smaller body of $\simeq 4$ km size would have an average polar tilt of $\simeq 40°$ per 100 My. Thus, if binary systems are typically old (ages $\gtrsim 100$ My), their poles might have been further evolved towards the YORP asymptotic states during their lifetime.

However, if the binary systems were systematically younger than inferred above from tidal evolution timescales, for instance because of their fast evolution due to the BYORP effect (e.g., Čuk and Burns 2004, Ćuk and Nesvorný 2010, McMahon and Scheeres 2010), the weak YORP torques on the primary would not have enough time to tilt the system orbital plane. In that case,

the concentration of binary orbit poles on high ecliptic latitudes would reflect primarily their *preferential formation* at these states (the hypothesis 1 above). As mentioned in the first paragraph of this section, during the YORP spin-up of parent bodies to the critical fission frequency, their spin orientations should be substantially YORP-tilted toward the YORP asymptotic states.

At this moment, the observations cannot discriminate between the two possibilities. More data and detailed theoretical understanding of the long-term binary evolution processes are needed to resolve this interesting issue.

Acknowledgements

APPENDIX

A Numerical model of binary's short-term evolution

In order to verify our conclusions in Sect. 5 we constructed a very simple numerical model to track orbital evolution of the binary system coupled with the spin evolution of the primary. The major simplifying assumptions are (i) a point-mass representation of the secondary component (the satellite), and (ii) an axisymmetric representation of the primary component of the binary system. Masses of the primary and secondary components are denoted

m_1 and m_2; we also define dimensionless factors $X_1 = m_1/(m_1 + m_2)$ and $X_2 = m_2/(m_1 + m_2)$, which correspond to their respective contributions to the total mass of the binary system.[9] The primary is assumed to be an oblate spheroid[10] with the equatorial and polar axes denoted by a_1 and c_1, such that $\gamma = c_1/a_1 \leq 1$. Denoting $R_1 \simeq a_1\gamma^{1/3}$ the characteristic radius of the primary, defined as a radius of a sphere with the same volume, and using R_1 as the scaling parameter of the representation of primary's gravitational field, we have $J_2 \simeq 0.2\,(1 - \gamma^2)\,\gamma^{-2/3}$ for its quadrupole parameter. We could also determine similar formulas for higher-degree zonal coefficients, but we shall not need them. Description of the evolution of the primary's spin axis also requires $(C - A)/C \simeq 0.5\,(1 - \gamma^2)$, where C and A are polar and equatorial moments of inertia. Photometric observations of the primary components in binaries, including those in this paper, all suggest a small amplitude of the lightcurve from which we may estimate the ratio of the equatorial axis is unity within $\simeq 10 - 20\%$ accuracy. Radar observations also support this conclusion and additionally suggest only modest polar flattening with $\gamma \simeq 0.8 - 0.9$ (e.g., Ostro et al. 2006, Shepard et al. 2006, Taylor et al. 2008, Benner et al. 2010). The mutual gravitational interaction of the primary and secondary components is represented in our model to the quadrupole level of the primary's zonal field; while we could have taken higher-degree zonal terms into account, they would not bring new qualitative features in our analysis.

On the contrary, we need to take into account effects of the solar gravity for the binary dynamics. We use description in Jacobi coordinates, where $\mathbf{r}$ denotes relative position vector of the secondary with respect to the primary and $\mathbf{R}$ denotes relative position vector of the Sun with respect to the center of mass of the binary. Since our prime concern is the evolution of $\mathbf{r}$, and the relative velocity $d\mathbf{r}/dt$, we represent $\mathbf{R}$ with a simple elliptic orbit. Because the secular evolution of the binary orbit plane may be coupled to the corresponding secular evolution of the heliocentric orbit plane of the binary's center-of-mass motion, we only pay attention to represent the inclination I and longitude of ascending node Ω evolutionary effects in $\mathbf{R}$ accurately enough. In particular, we use a Fourier representation of the non-singular inclination vector $\zeta = q + \imath p = \sin I/2 \exp(\imath\Omega)$, in which we retain the two dominant terms: the proper term with frequency s and the forced terms with frequency s_6 (see, e.g., Vokrouhlický et al. 2006). In the case of binaries on high-inclination heliocentric orbits, such as those in the Hungaria or Phocaea groups, it is necessary to include also additional forced terms due to the terrestrial planets such as s_3 and s_4, because they are more important than the s_6 term and their frequencies are close to s (e.g., Milani et al. 2010). All these harmonic terms were obtained by numerically integrating the heliocentric orbit of the binary over 10 My time interval, and Fourier analysing of the osculating $\zeta = q + \imath p$ values.

---

[9] Masses of both components were computed from the estimated sizes in Table 1 and a bulk density of 2.5 g/cm^3.

[10] The exact nature of the shape is, however, not a very restrictive assumption. As mentioned above, the major approximation in our model is the axial symmetry of the primary.

With these assumptions, the relative vector $\mathbf{r}$ satisfies

$$\frac{d^2\mathbf{r}}{dt^2} + G\,\frac{m_1 + m_2}{r^3}\,\mathbf{r} = Gm_0 \left[\left(\frac{1}{\Delta_{20}^3} - \frac{1}{\Delta_{10}^3} \right) \mathbf{R} - \left(\frac{X_1}{\Delta_{20}^3} + \frac{X_2}{\Delta_{10}^3} \right) \mathbf{r} \right]$$

$$+ \frac{3\,G\,(m_1 + m_2)}{2\,r^5} \left(\frac{R_1}{r} \right)^2 J_2 \left\{ \left[5\,(\mathbf{r}\cdot\mathbf{s})^2 - r^2 \right] \mathbf{r} - 2r^2\,(\mathbf{r}\cdot\mathbf{s})\,\mathbf{s} \right\} \ , \text{(A.1)}$$

where m_0 is the solar mass, $\Delta_{10}^2 = R^2 + 2\,X_2\,(\mathbf{r}\cdot\mathbf{R}) + X_2^2 r^2$ and $\Delta_{20}^2 = R^2 - 2\,X_1\,(\mathbf{r}\cdot\mathbf{R}) + X_1^2 r^2$ are mutual distances of the primary and the secondary components in the binary to the Sun, and $\mathbf{s}$ is the direction of the spin vector of primary. The latter evolves due to gravitational torques exerted by the satellite and the Sun, and we have

$$\frac{d\mathbf{s}}{dt} = \frac{3\,Gm_2}{r^5\omega}\,\frac{C - A}{C}\,(\mathbf{r}\cdot\mathbf{s})\,(\mathbf{r}\times\mathbf{s}) + \frac{3\,Gm_0}{R^5\omega}\,\frac{C - A}{C}\,(\mathbf{R}\cdot\mathbf{s})\,(\mathbf{R}\times\mathbf{s}) \ , \quad \text{(A.2)}$$

where ω is the angular rotation frequency of the primary (constant in our model). Here, the first term is the satellite's torque and the second term is the Sun's torque. Because $r \ll R$, the satellite's term "nominally dominates", but if the satellite is very close to the primary's equator the solar term also contributes. Obviously, for a spherical primary ($\gamma = 1$ and thus $(C - A)/C = 0$) the spin $\mathbf{s}$ is fixed and the relative orbit of the binary evolves as in the point-mass problem.

Equations (A.1) and (A.2) are numerically propagated using a Burlish-Stoer scheme with variable timestep complying to a chosen accuracy level (e.g., Press et al. 2007). Therefore, our characteristic timestep is typically a fraction of hour. The initial data for $(\mathbf{r}, d\mathbf{r}/dt, \mathbf{s})$ correspond to a near-circular orbit in the equatorial plane of the primary (thus $\mathbf{s} \parallel \mathbf{r}\times d\mathbf{r}/dt$; for sake of simplicity we did not explore solutions with the satellite orbit inclined to the primary's equator). Its semimajor axis a_{orb} is determined by the observed orbital period P_{orb} in Table 1. The initial orientation of the primary spin axis $\mathbf{s}$ is either determined by the orbital pole from Table 1, or we run a sample of simulations with several initial latitudes in order to test short-term stability of the solution: $B_{\mathrm{p}} = 0°$, $B_{\mathrm{p}} = \pm 20°$, $B_{\mathrm{p}} = \pm 40°$, $B_{\mathrm{p}} = \pm 60°$ and $B_{\mathrm{p}} = \pm 80°$. We still have to select the initial ecliptic longitude L_{p} of $\mathbf{s}$: given the possible circulation of $\mathbf{s}$ about the Cassini states related to the precessing orbit, we choose $L_{\mathrm{p},1} = \Omega + 90°$ and $L_{\mathrm{p},2} = \Omega + 270°$. Intermediate values of L_{p} would lead to solutions that are represented as a composition of the chosen cases. For definiteness, we choose the primary geometrical oblateness $\gamma = 0.89$, which is the value determined for the best studied binary case of (66391) 1999 KW4 (Ostro et al. 2006); however, our results and conclusions are not overly sensitive to this value. Our model is only adequate to describe the binary evolution over a moderate timescale, but is fundamentally incomplete to represent a long-term evolution. For that reason we set the maximum time of integration to 500 ky. Obviously, we also stop the simulation when the distance r of the primary and secondary components would become: (i) smaller than sum of their radii (estimated in

Table 1), or (ii) larger than the estimated Hill radius of their gravitational interaction (typically few hundreds of primary radii).

As demonstrated in Sect. 5, the oblateness of the primary efficiently couples the evolution of its spin axis $\mathbf{s}$ and the binary orbital angular momentum $(m_1 + m_2)\, X_1 X_2\, \mathbf{r} \times (d\mathbf{r}/dt)$ for compact systems (i.e., when $r \ll d_2$ from footnote 4). In this situation, the orbit pole evolution may be obtained by numerical integration of a much simpler system

$$\frac{d\mathbf{s}'}{dt} = -\left[\alpha_{\mathrm{eff}}\,(\mathbf{n}\cdot\mathbf{s}')\,\mathbf{n} + \boldsymbol{\sigma}\right] \times \mathbf{s}' , \tag{A.3}$$

where $\mathbf{s}'$ is the primary and orbit pole referred to the system of axes precessing with the binary's heliocentric orbit, such that the x-axis is rotated in the osculating plane by $-\Omega$ from the ascending node and the z-axis is along the osculating normal $\mathbf{n}$ to the heliocentric orbital plane, α_{eff} is the effective precession constant from Eq. (11) and $\boldsymbol{\sigma} = (\sigma_1, \sigma_2, -2\sigma_3)^T$, with

$$\sigma_1 = \cos\Omega\,(dI/dt) - \sin I \sin\Omega\,(d\Omega/dt) , \tag{A.4}$$
$$\sigma_2 = \sin\Omega\,(dI/dt) + \sin I \cos\Omega\,(d\Omega/dt) , \tag{A.5}$$
$$\sigma_3 = \sin^2 I/2\,(d\Omega/dt) . \tag{A.6}$$

Here, I and Ω are the osculating values of inclination and longitude of ascending node of the binary heliocentric orbit, and dI/dt and $d\Omega/dt$ are their rates induced by planetary perturbations. Not only the system (A.3) is much simpler than Eqs. (A.1) and (A.2), but most importantly it eliminates orbital motion of the binary. As a result, the shortest timescale involved is that of secular evolution of the binary's heliocentric orbit and consequently one can take a much longer integration timestep. Additionally, an efficient Lie-Poisson integration scheme is available for this system (e.g., Breiter et al. 2005), which optimizes the integrator speed. Therefore a sample of binary's orbit-pole evolution can be efficiently obtained by integration of (A.3). The scheme may even contain a slow, adiabatic, evolution of the binary orbit induced by tides or BYORP effects (e.g., Taylor and Margot 2010, 2011, Ćuk and Burns 2004, Ćuk and Nesvorný 2010, McMahon and Scheeres 2010). In this case the precession constant α_{eff} would slowly evolve, reflecting slow changes in the satellite orbit.

References

Benner, L.A.M., et al., 2010. Radar imaging and a physical model of binary asteroid 65803 Didymos. Bull. Am. Astron. Soc. 42, 1056.

Bertotti, B., Farinella, P., Vokrouhlický, D., 2003. Physics of the Solar System (Kluwer Academic Publishers, New York).

Bottke, W.F., et al., 2005. Linking the collisional history of the main asteroid belt to its dynamical excitation and depletion. Icarus 179, 63–94.

Bottke, W.F., Vokrouhlický, D., Rubincam, D.P., Nesvorný, D., 2006. The Yarkovsky and YORP effects: Implications for asteroid dynamics. Annu. Rev. Earth Planet. Sci. 34, 157–191.

Breiter, S., Elipe, A., 2006. Critical inclination in the main problem of a massive satellite. Celest. Mech. Dyn. Astron. 95, 287–297.

Breiter, S., Nesvorný, D., Vokrouhlický, D., 2005. Efficient Lie-Poisson integrator for secular spin dynamics of rigid bodies. Astron. J. 130, 1267–1277.

Carruba, V., Burns, J.A., Nicholson, P.D., Gladman, B.J., 2002. On the inclination distribution of the Jovian irregular satellites. Icarus 158, 434–449.

Colombo, G., 1966. Cassini's second and third laws. Astron. J. 71, 891–896.

Čapek, D., Vokrouhlický, D., 2004. The YORP effect with finite thermal conductivity. Icarus 172, 526–536.

Ćuk, M., Burns, J.A., 2004. Effects of thermal radiation on the dynamics of binary NBAs. Icarus 176, 418–431.

Ćuk, M., Nesvorný, D., 2010. Orbital evolution of small binary asteroids. Icarus 207, 732–743.

French, R.G., et al., 1993. Geometry of the Saturn system from the 3 July 1989 occultation of 28 Sgr and Voyager observations. Icarus 103, 163–214.

Goldreich, P., 1965. Inclination of satellite orbits about an oblate precessing planet. Astron. J. 70, 5–9.

Hanuš, J., et al., 2011. A study of asteroid pole-latitude distribution based on an extended set of shape models derived by the lightcurve inversion method. Astron. Astrophys. 530, A134.

Henrard, J., Murigande, C., 1987. Colombo's top. Celest. Mech. 40, 345–366.

Kaasalainen, M., Torppa, J., Muinonen, K., 2002. Models of twenty asteroids from photometric data. Icarus 159, 369–395.

Kozai, Y., 1962. Secular perturbations of asteroids with high inclination and eccentricity. Astron. J. 67, 591–598.

Jacobson, S.A., Scheeres, D.J., 2011. Dynamics of rotationally fissioned asteroids: Source of observed small asteroid systems. Icarus 214, 161–178.

McMahon, J., Scheeres, D.J., 2010. Detailed prediction for the BYORP effect on binary near-Earth Asteroid (66391) 1999 KW4 and implications for the binary population. Icarus 209, 494–509.

Mignard, F., 1981. Evolution of the Martian satellites. Mon. Not. Roy. Astron. Soc. 194, 365–379.

Milani, A., Knežević, Z., Novaković, B., Cellino, A., 2010. Dynamics of the Hungaria asteroids. Icarus 207, 769–794.

Murray, C.D., Dermott, S.F., 1999. Solar System Dynamics. Cambridge University Press

Nesvorný, D., Alvarellos, J.L.A., Dones, L., Levison, H.F., 2003. Orbital and collisional evolution of the irregular satellites. Astron. J. 126, 398–429.

Ostro, S.J., et al., 2006. Radar imaging of binary near-Earth asteroid (66391) 1999 KW4. Science 314, 1276–1280.

Pravec, P., Harris, A.W., 2007. Binary asteroid population. 1. Angular momentum content. Icarus 190, 250–259.

Pravec, P., et al., 2005. Tumbling asteroids. Icarus 173, 108–131.

Pravec, P., et al., 2006. Photometric survey of binary near-Earth asteroids. Icarus 181, 63–93.

Press, W.H., Teukolsky, S.A., Vetterling, W.T., Flannery, B.P., 2007. Numerical Recipes (Cambridge University Press, Cambridge)

Scheeres, D.J., 2007. Rotational fission of contact binary asteroids. Icarus 189, 370–385.

Scheirich, P., Pravec, P., 2009. Modeling of lightcurves of binary asteroids. Icarus 200, 531–547.

Shepard, M.K., et al., 2006. Radar and infrared observations of binary near-Earth asteroid 2002 CE26. Icarus 184, 198–210.

Stephens, R.D., Warner, B.D., Harris, A.W., 2010. A proposed standard for reporting asteroid lightcurve data. Bull. Amer. Astron. Soc. 42, 1035.

Taylor, P.A., Margot, J.-L., 2010. Tidal evolution of close binary asteroid systems. Celest. Mech. Dyn. Astr. 108, 315–338.

Taylor, P.A., Margot, J.-L., 2011. Binary asteroid systems: Tidal end states and estimates of material properties. Icarus 212, 661–676.

Taylor, P.A., et al., 2008. The shape, mutual orbit, and tidal evolution of binary near-Earth asteroid 2004 DC. LPIC 1405, 8322.

Tedesco, E.F., Noah, P.V., Noah, M., Price, S.D., 2002. The Supplemental IRAS Minor Planet Survey. Astron. J. 123, 1056–1085.

Vokrouhlický, D., Nesvorný, D., Bottke, W.F., 2006. Secular spin dynamics of inner main-belt asteroids. Icarus 184, 1–28.

Walsh, K.J., Richardson, D.C., Michel, P., 2008. Rotational breakup as the

origin of small binary asteroids. Nature 454, 188–191.

Ward, W.R., 1975. Tidal friction and generalized Cassini's laws in the solar system. Astron. J. 80, 64–70.

Warner, B.D., Harris, A.W., Pravec, P., 2009a. An analysis of slow rotators among the Hungaria asteroids. Bull. Amer. Astron. Soc. 41, 1062.

Warner, B.D., Harris, A.W., Pravec, P., 2009b. The asteroid lightcurve database. Icarus 202, 134–146.

Warner, B.D., Harris, A.W., Vokrouhlický, D., Nesvorný, D., Bottke, W.F., 2009c. Analysis of the Hungaria asteroid population. Icarus 204, 172–182.

Table 1: Parameters of 18 binary asteroids observed in more than one apparition

Binary system	Apparitions	D_1(km)	D_2/D_1	P_1(h)	P_{orb}(h)	P_2(h)	a_{orb}/D_1	L_{p} (°)	B_{p} (°)	ϵ (°)	$(a_1/c_1)_{\mathrm{max}}$	e_{max}	a_{h}(AU)	i_{h}(°)
(1338) Duponta	07, 10	7.4	0.24	3.85453	17.5680	(17.57)	2.0	0 - 360	+66 - +90	0 - 21	3.3^a	0.14 (07)	2.264	4.82
			±.02	±.00009	±.0001	±.01								
(1453) Fennia	07, 09, 11	7.0	0.28	4.4121	23.00351		2.6	89 - 118	−70 - −62	172 - 180	2.4^b	0.03 (11)	1.897	23.68
			±.02	±.0003	±.00005									
(1830) Pogson	07, 08, 10	7.8	(0.30)	2.57003	24.24580		(2.5)	130 - 274	−86 - −74	162 - 180	3.4^c	0.10 (08)	2.188	3.95
			±.02	±.00006	±.00006									
(2006) Polonskaya	05, 08, 10	5.5	(0.23)	3.1180	19.153^d		(2.1)						2.325	4.92
			±.03	±.0001										
(2044) Wirt	05/06, 08, 10^e	5.6	0.25	3.6897	18.976	(18.97)	2.1	349 - 23	−72 - −52	120 - 143^f	1.5	0.10 (05)	2.380	23.98
			±.02	±.0003	±.005	±.02								
(2 pole solutions)					18.965			168 - 203	+58 - +72	37 - 53				
					±.006									
(2577) Litva	09, 10	4.0	(0.34)	2.81292	35.8723		(3.2)	253 - 348	−84 - −68	158 - 178	2.3	0.08 (09)	1.904	22.91
			±.02	±.00009	±.0008									
(2754) Efimov	06, 08, 11	4.9	0.22	2.44967	14.77578		1.8	0 - 360	−90 - −66	154 - 180	1.8^a	0.08 (06)	2.228	5.71
			±.02	±.00002	±.00008									
(3309) Brorfelde	05, 09, 10	4.7	0.26	2.5042	18.46444	18.45	2.0	116 - 154	−74 - −64	168 - 180	2.1^c	0.08 (10)	1.817	21.14
			±.02	±.0002	±.00003	±.02								
(3868) Mendoza	09, 10	8.3	0.17	2.77089	12.1944		1.5						2.333	8.10
			±.02	±.00005	±.00008									
(4029) Bridges	06, 07, 10	7.7	0.27	3.5750	16.31701		1.9	0 - 360	−90 - −62	157 - 180	3.5	0.17 (06)	2.525	5.44
			±.03	±.0004	±.00004									
(5477) Holmes	05, 07	2.9	0.39	2.9940	24.4036	(24.41)	2.5	320 - 332	+38 - $+64^g$	5 - 30^g	2.0^h	0.05 (05)	1.917	22.55
			±.02	±.0002	±.0002	±.01								
(5905) Johnson	05, 08	3.6	0.38	3.7823	21.75639		2.3	30 - 58	+60 - +76	0 - 14	2.3	0.13 (05)	1.910	27.52
			±.02	±.0002	±.00006									
(2 pole solutions)					21.79699			210 - 254	−56 - −76	167 - 180				
					±.00009									
(6084) Bascom	05/06, 08^i	5.8	0.37	2.7453	43.51	(43.5)	3.7	267 - 378	−76 - −56	127 - 169	2.9	0.15 (06)	2.313	23.01
			±.02	±.0002	±.02	±.1								
(6244) Okamoto	06, 09	4.4	0.25	2.8957	20.3105		2.2	0 - 360	+54 - $+90^j$	0 - 33^j	3.0^k	0.15 (06)	2.160	5.40
			±.02	±.0003	±.0002									
(2 pole solutions)					20.3232			0 - 360	−90 - $−58^l$	151 - 180^l				
					±.0002									
(6265) 1985 TW3	07, 10	5.2	(0.32)	2.7092	15.86^m		1.9						2.166	4.11
			±.02	±.0001										
(9617) Grahamchapman	06, 08	2.8	(0.27)	2.28561	19.3817		2.1	0 - 360	+48 - $+90^n$	0 - 38^n	2.4^k	0.19 (06)	2.224	6.14
			±.03	±.00006	±.0004									
(2 pole solutions)					19.3915			0 - 360	−90 - $−50^p$	141 - 180^p				
					±.0004									

Table 1: *cont.*

Binary system	Apparitions	D_1(km)	D_2/D_1	P_1(h)	P_{orb}(h)	P_2(h)	a_{orb}/D_1	L_p (°)	B_p (°)	ϵ (°)	$(a_1/c_1)_{max}$	e_{max}	a_h(AU)	i_h(°)
(17260) 2000 JQ58	06, 09	3.2	0.26	3.1287	14.7577	14.745	1.8	0 - 360	−90 - −56^q	147 - 180^q	2.2	0.20 (06)	2.204	5.28
			±.03	±.0001	±.0002	±.003								
(2 pole solutions)					14.7523				0 - 360	+46 - +90^r	0 - 43^r				
					±.0003									
(76818) 2000 RG79	05, 08/09	2.8	(0.35)	3.1665	14.11960	14.127	1.7	28 - 360	+72 - +90	0 - 22	1.7^k	0.13 (08)	1.930	18.13
			±0.02	±.0002	±.00007	±.002								
(2 pole solutions)					14.12998				0 - 360	−90 - −70	158 - 180				
					±.00005									

The listed parameters are: the mean diameter of the primary at the equatorial aspect (D_1), estimated from the measured absolute magnitude (H) at the system's mean light and an assumed geometric albedo based on family or orbital group membership according to Warner et al. (2009b) or, in the case of 1453 Fennia, estimated in Tedesco et al. (2002), using the method in Pravec and Harris (2007); the ratio between the mean diameters of the components of the binary (D_2/D_1); the rotation period of the primary (P_1); the orbit period (P_{orb}), the rotation period of the secondary (P_2); the relative size of the mutual orbit's semi-major axis (a_{orb}/D_1); ranges of admissible values of the mutual orbit pole's ecliptic longitude, latitude, and obliquity to the current heliocentric orbit (L_p, B_p, ϵ); the upper limit on the equatorial-to-polar axis ratio of the primary; the upper limit on eccentricity of the mutual orbit, estimated from the apparition specified in parentheses; the semi-major axis (a_h) and inclination (i_h) of the system's heliocentric orbit (epoch 2011 Aug. 27.0 TT).

See the electronic files available at http://www.asu.cas.cz/~asteroid/binastdata.htm for references, comments, additional estimated parameters, and uncertainties.

Values in parentheses have following meanings: the estimated size ratios D_2/D_1 may be only lower limits, as the assumption of that we observed total events or that a possible third component has a negligible size may not hold; the secondary period (P_2) solutions are likely but not entirely unique; and the estimates of the relative semi-major axis a_{orb}/D_1 may be affected by presence of the possible third component.

^{a} The best-fit value is 1.1, and the quality of the fit decreases with increasing a_1/c_1, so the lower values are preferred.

^{b} Lower limit on a_1/c_1 is 1.4.

^{c} The best-fit value is 1.3, and the quality of the fit decreases with increasing a_1/c_1, so the lower values are preferred.

^{d} There are five discrete solutions, see text.

^{e} Mutual events were observed in the first apparition only. In the two return apparitions, there did not occur mutual events with depth greater than 0.03 mag. We modeled the orbital lightcurve component from the first apparition only.

^{f} Quality of the fit decreases with decreasing ϵ, so the higher values are preferred.

^{g} Model bulk density increases from 0.8 to 1.9 g cm^{-3} with increasing B_p. The most plausible solution is for $B_p \sim +60°$ and $\epsilon \sim 8°$.

^{h} The best-fit value is 1.2, and the quality of the fit decreases with increasing a_1/c_1, so the lower values are preferred.

^{i} In the return apparition, there did not occur mutual events width depth greater than 0.02 mag. We modeled the orbital lightcurve component from the first apparition only. The lack of mutual events in the return apparition did not constrain the solution further; for all poles within the area derived from the first apparitions, there do not occur events for the geometry of the return apparition.

^{j} For model bulk density > 1.0 g cm^{-3} the values of B_p and ϵ are constrained to be > +64° and < 21°, respectively.

^{k} The best-fit value is 1.0, and the quality of the fit decreases with increasing a_1/c_1, so the lower values are preferred.

^{l} For model bulk density > 1.0 g cm^{-3} the values of B_p and ϵ are constrained to be < −66° and > 159°, respectively.

^{m} There are four discrete solutions in a range from 15.84 to 15.87 h.

^{n} For model bulk density > 1.0 g cm^{-3} the values of B_p and ϵ are constrained to be > +62° and < 24°, respectively.

^{p} For model bulk density > 1.0 g cm^{-3} the values of B_p and ϵ are constrained to be < −62° and > 156°, respectively.

^{q} For model bulk density > 1.0 g cm^{-3} the values of B_p and ϵ are constrained to be < −62° and > 153°, respectively.

^{r} For model bulk density > 1.0 g cm^{-3} the values of B_p and ϵ are constrained to be > +62° and < 27°, respectively.

Table 2

Epochs of mutual events in the discovery and the return apparitions for the 18 binaries. The data for the first positive event detection in each apparition are listed.

Binary system	Date (UT)	$L(°)$	$B(°)$	$L_h(°)$	$B_h(°)$	EventDet
(1338) Duponta	2007-03-06.9	160.1	-2.5	162.7	-1.4	P
(1338) Duponta	2010-01-05.0	82.0	7.2	92.7	3.9	P
(1453) Fennia	2007-11-04.4	76.8	33.9	58.7	18.9	P
(1453) Fennia	2009-08-14.6	293.1	-39.5	309.3	-20.4	P
(1830) Pogson	2007-04-18.6	220.6	6.7	214.8	3.6	P
(1830) Pogson	2010-02-20.7	183.7	2.6	169.3	1.5	P
(2006) Polonskaya	2005-11-01.2	46.9	6.8	42.6	3.3	P
(2006) Polonskaya	2008-06-05.3	294.3	-7.7	278.4	-4.9	N
(2044) Wirt	2005-12-05.9	56.5	13.7	66.8	5.7	P
(2044) Wirt	2008-08-24.3	316.7	-35.5	322.3	-24.0	N
(2577) Litva	2009-03-02.2	132.3	-28.2	149.4	-13.0	P
(2577) Litva	2010-08-11.3	335.4	25.6	327.1	13.8	P
(2754) Efimov	2006-08-14.2	0.9	10.6	339.1	5.1	P
(2754) Efimov[a]	2011-01-31.0	139.2	-6.2	135.8	-3.7	P
(3309) Brorfelde	2005-10-25.2	21.1	-2.5	26.7	-1.2	P
(3309) Brorfelde	2009-01-28.3	147.4	39.6	136.7	20.3	P
(3868) Mendoza	2009-04-25.5	221.4	10.0	218.9	6.0	P
(3868) Mendoza	2010-09-07.0	25.2	-3.6	6.9	-2.1	P
(4029) Bridges	2006-04-11.6	222.3	-0.3	213.0	-0.2	P
(4029) Bridges	2007-10-06.0	356.8	4.6	2.5	2.9	P
(5477) Holmes	2005-11-02.3	47.0	-5.3	43.2	-2.5	P
(5477) Holmes	2007-06-10.5	225.7	-10.7	242.7	-5.6	P
(5905) Johnson	2005-04-01.3	185.4	38.8	188.7	20.9	P
(5905) Johnson	2008-05-13.4	279.3	43.6	254.3	25.6	P
(6084) Bascom	2005-12-29.6	139.5	-18.4	120.5	-10.9	P
(6084) Bascom	2008-09-01.6	351.8	-15.2	345.4	-7.5	N
(6244) Okamoto	2006-09-26.2	2.9	6.2	2.9	2.8	P
(6244) Okamoto	2009-08-14.6	320.3	-2.0	321.1	-1.0	P
(6265) 1985 TW3	2007-07-15.5	297.4	-8.8	294.6	-3.9	P
(6265) 1985 TW3	2010-06-13.6	244.8	-4.0	253.7	-2.0	P
(9617) Grahamchapman	2006-01-27.3	139.3	-6.3	133.4	-3.3	P
(9617) Grahamchapman	2008-12-26.2	63.7	-11.3	78.7	-6.1	P
(17260) 2000 JQ58	2006-01-29.6	148.0	-10.0	138.0	-4.7	P
(17260) 2000 JQ58	2009-01-01.3	65.0	-8.8	82.8	-4.7	P
(76818) 2000 RG79	2005-08-07.3	342.2	21.1	327.9	10.8	P
(76818) 2000 RG79	2008-10-03.4	73.3	28.3	41.3	17.2	P

The ecliptic coordinates are in the equinox of J2000. For definition of positive/negative (P/N) event detection, see text.

[a] We observed Efimov in the 2nd apparition of March 2008 when the asteroid was placed almost precisely (within a few degrees) diametrically opposite in its heliocentric orbit with respect to the discovery apparition. As such, the 2008 apparition's data would provide negligible constraints in the simulations presented in Section 4 and therefore we did not count the 2008 apparition as a fully-fledged return apparition for the purpose of the survey simulations. Instead, we took the 2011 apparition as the return apparition.

Table 3

Results of the simulations of the binary survey for two assumed distributions of orbit poles: the isotropic distribution (columns 4–6) and the uniform distribution in $|\cos \epsilon|$ from $\sin 60°$ to 1 (columns 7–9).

| Binary system | $\sin i_c$ | $\alpha(°)$ | isotropic | | | $\epsilon_x = 30°$ | | |
			n_{1stapp}	n_{2ndapp}	Prob. $(\frac{n_{2ndapp}}{n_{1stapp}})$	n_{1stapp}	n_{2ndapp}	Prob. $(\frac{n_{2ndapp}}{n_{1stapp}})$
(1338) Duponta	0.310	2.8	7617	1286	0.169	17841	9644	0.541
(1453) Fennia	0.246	22.0	9985	2963	0.297	20930	16502	0.788
(1830) Pogson	0.260	6.4	7152	1749	0.245	16554	11168	0.675
(2006) Polonskaya	0.293	5.5	7492	1406	0.188	17767	10562	0.594
(2044) Wirt	0.298	12.9	8913	2212	0.248	21897	15991	0.730
(2577) Litva	0.209	22.0	8988	6620	0.737	18403	18010	0.979
(2754) Efimov	0.339	22.3	10934	4469	0.409	20798	16221	0.780
(3309) Brorfelde	0.315	5.7	8264	2491	0.301	18616	14393	0.773
(3868) Mendoza	0.390	4.7	8983	3494	0.389	20908	15806	0.756
(4029) Bridges	0.334	9.3	9269	2927	0.316	19674	15230	0.774
(5477) Holmes	0.278	4.8	7565	6091	0.805	18499	16036	0.867
(5905) Johnson	0.300	18.1	10208	3826	0.375	23887	20276	0.849
(6084) Bascom	0.185	19.9	7606	1390	0.183	18081	8266	0.457
(6244) Okamoto	0.284	3.4	7073	1567	0.222	17234	10906	0.633
(6265) 1985 TW3	0.347	5.7	9001	2631	0.292	21888	16779	0.767
(9617) Grahamchapman	0.302	6.6	8156	1644	0.202	18691	12142	0.650
(17260) 2000 JQ58	0.350	11.3	10014	2201	0.220	21938	16091	0.733
(76818) 2000 RG79	0.397	17.2	12519	3814	0.305	25207	22198	0.881

Note: In columns 2 and 3, the values of $\sin i_c$ and the solar phase of the first positive event observation are listed. A correlation of n_{1stapp} for the isotropic distribution with both $\sin i_c$ and the solar phase is apparent; as given in Section 2, the mean probability of the event detection is equal to $\sin i_c$ (eq. 7) at zero solar phase, increased at higher solar phases, and further modified by the event resolving probability function p_{res} (not illustrated here).
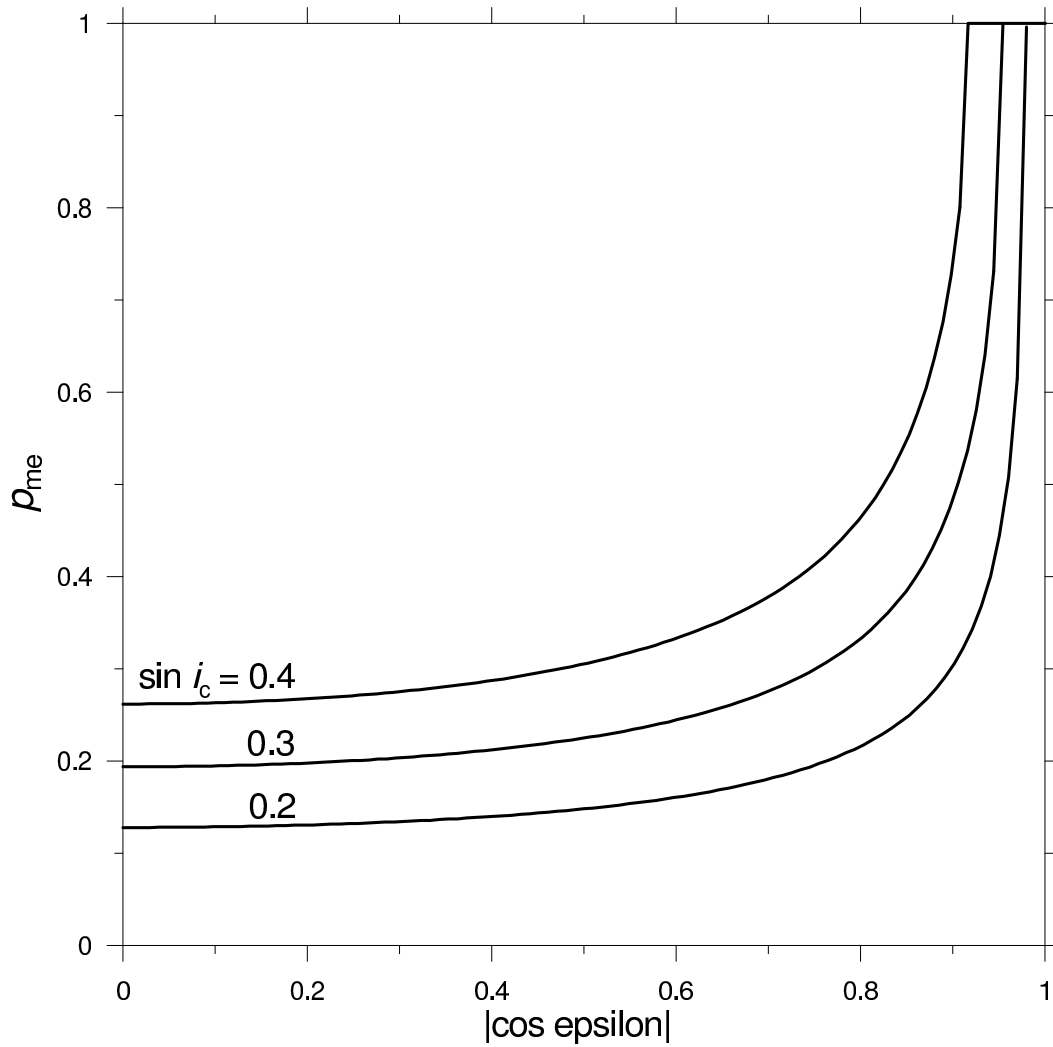
Fig. 1. A dependence of the probability of occurrence of mutual events on the cosine of obliquity for three values of $\sin i_c$ for the special case of a binary system with spherical components, zero eccentricity of the mutual orbit, and observed at zero solar phase.
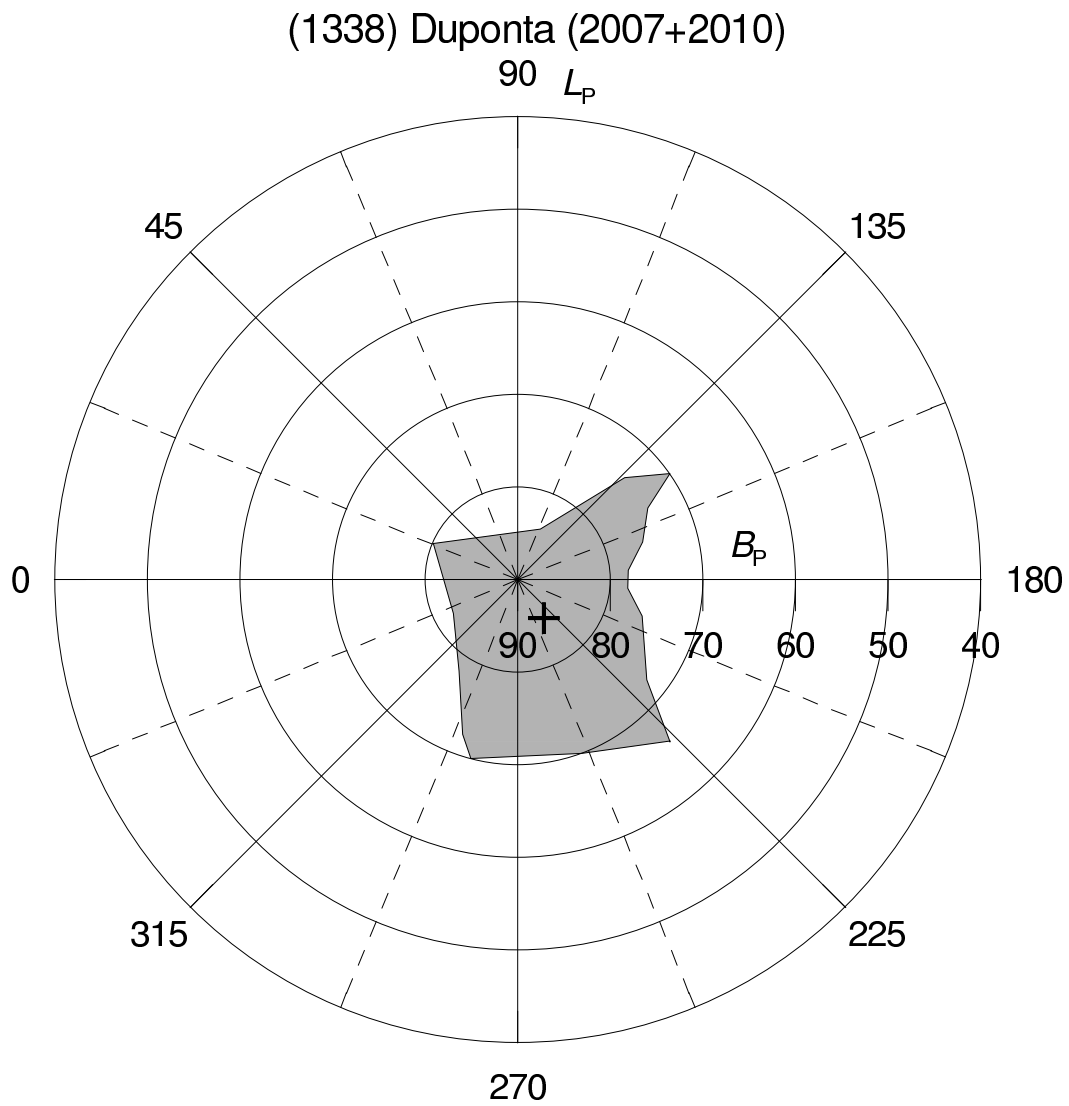
Fig. 2. Area of admissible poles for the mutual orbit of (1338) Duponta in ecliptic coordinates. The north pole of the current asteroid's heliocentric orbit is marked with the cross. This area corresponds to 3σ confidence level.
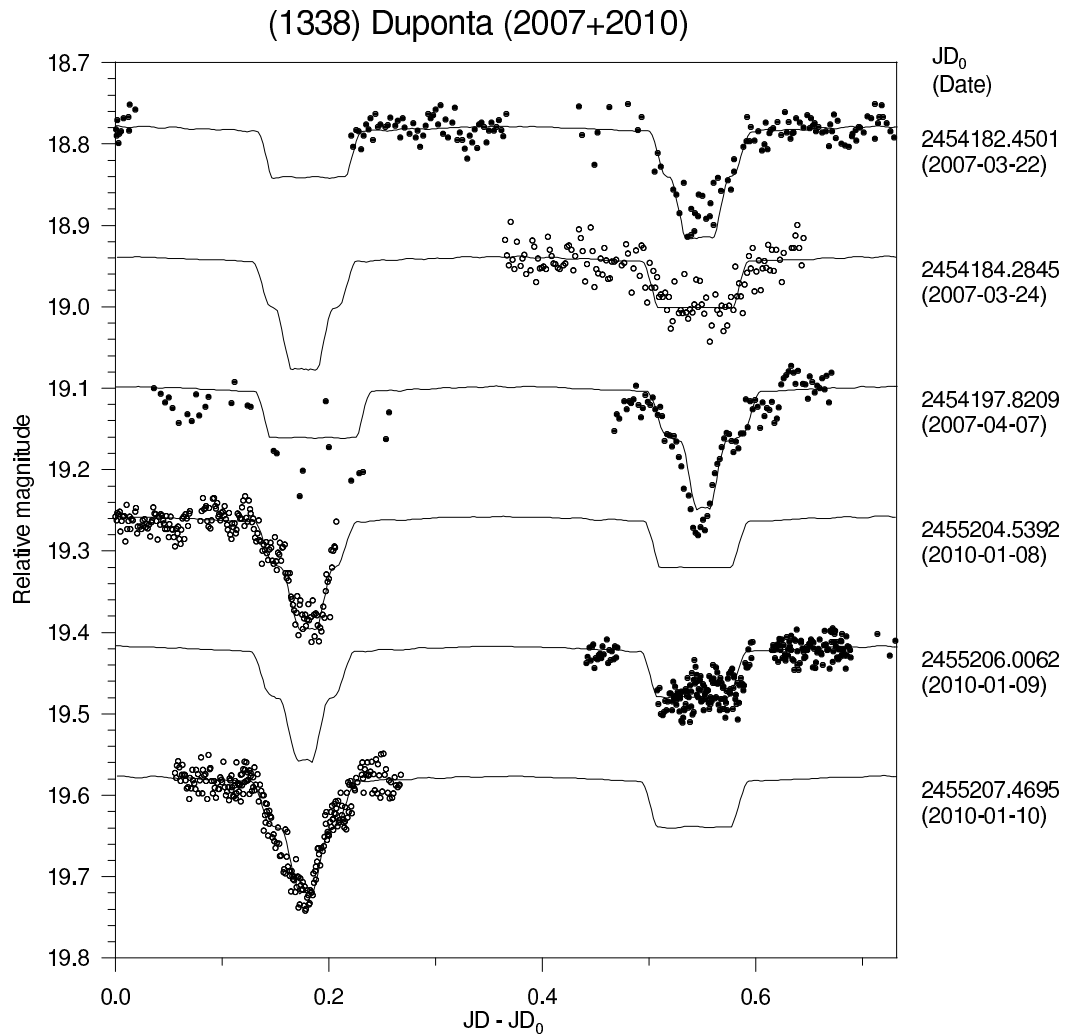
Fig. 3. Sample of the orbital lightcurve component's data of (1338) Duponta in apparitions 2007 and 2010. The observational data (points) are plotted together with the synthetic lightcurve for the best-fit solution (curve). The data sets from different dates are vertically offset for clarity, and different symbols are used for them to avoid confusion. The epochs of the origins of each curve (JD_0) are listed in the right column. On the first and third curves from the top, the minima are shown in an order opposite (i.e., first the secondary and then the primary event) to the other curves.
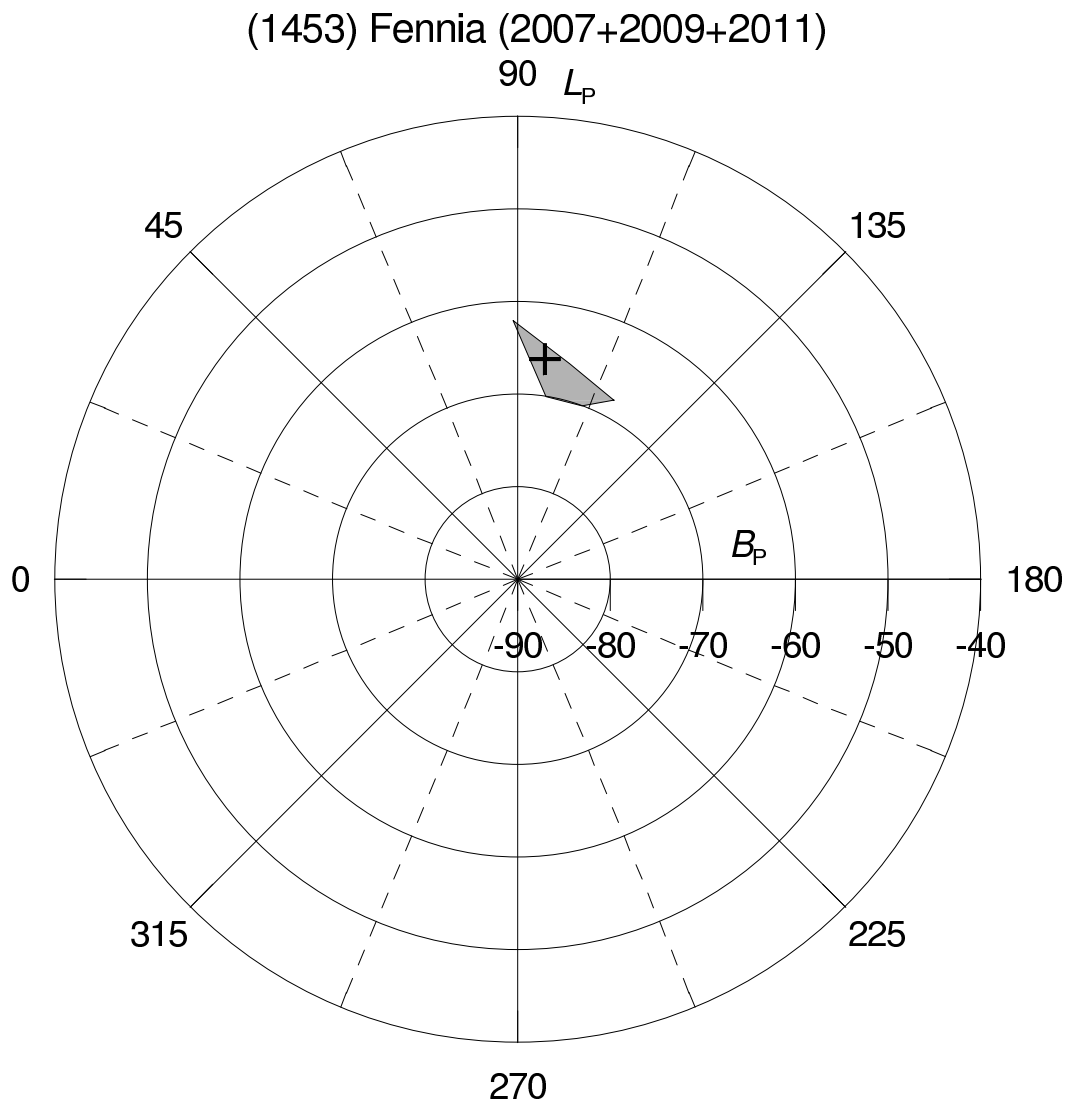
Fig. 4. Area of admissible poles for the mutual orbit of (1453) Fennia in ecliptic coordinates. The south pole of the current asteroid's heliocentric orbit is marked with the cross.
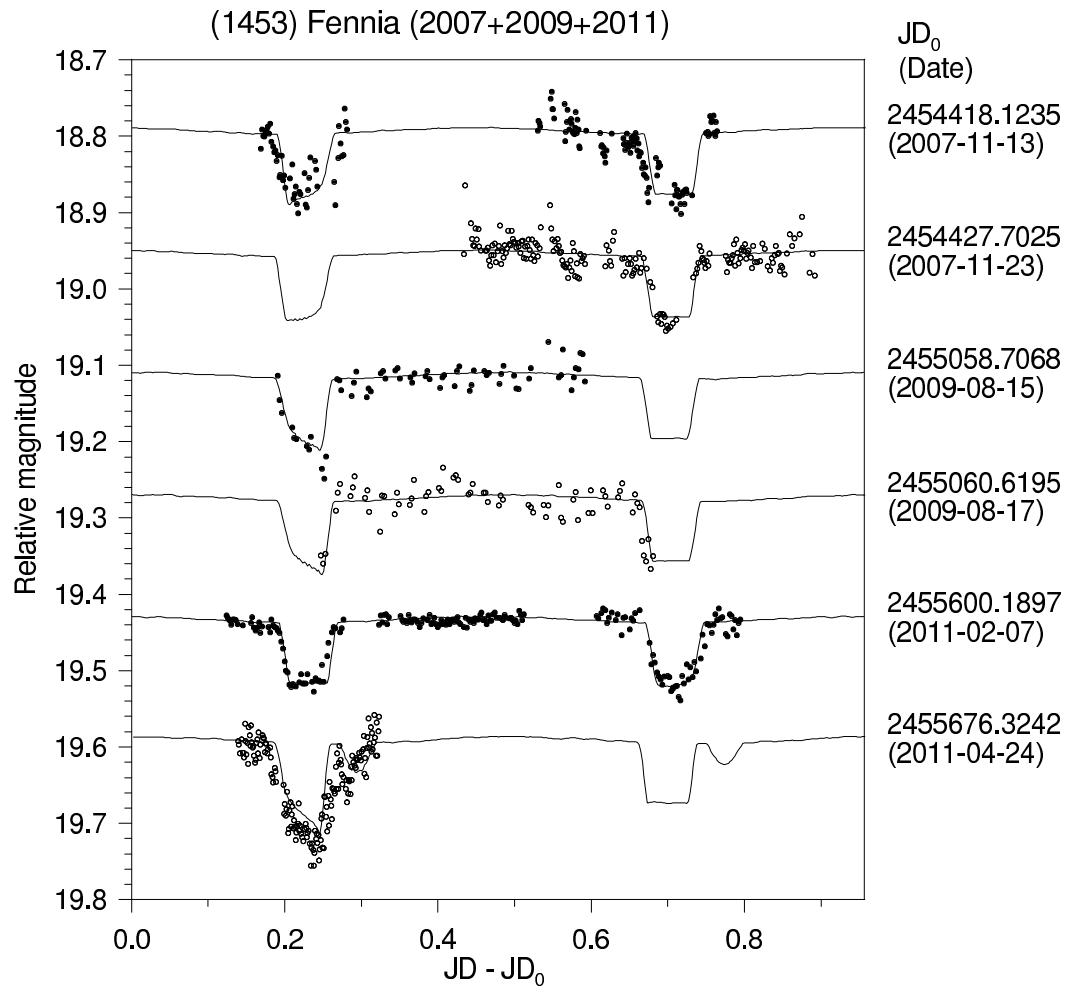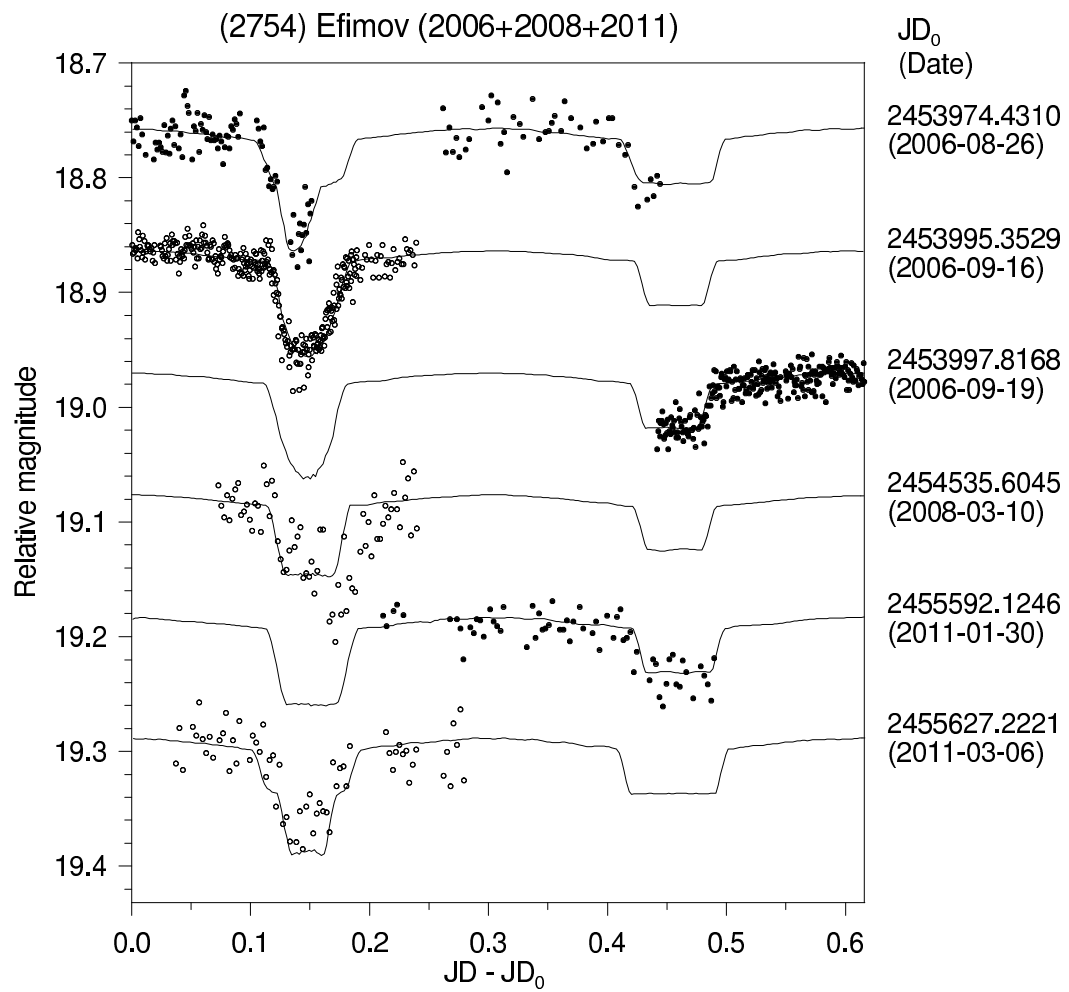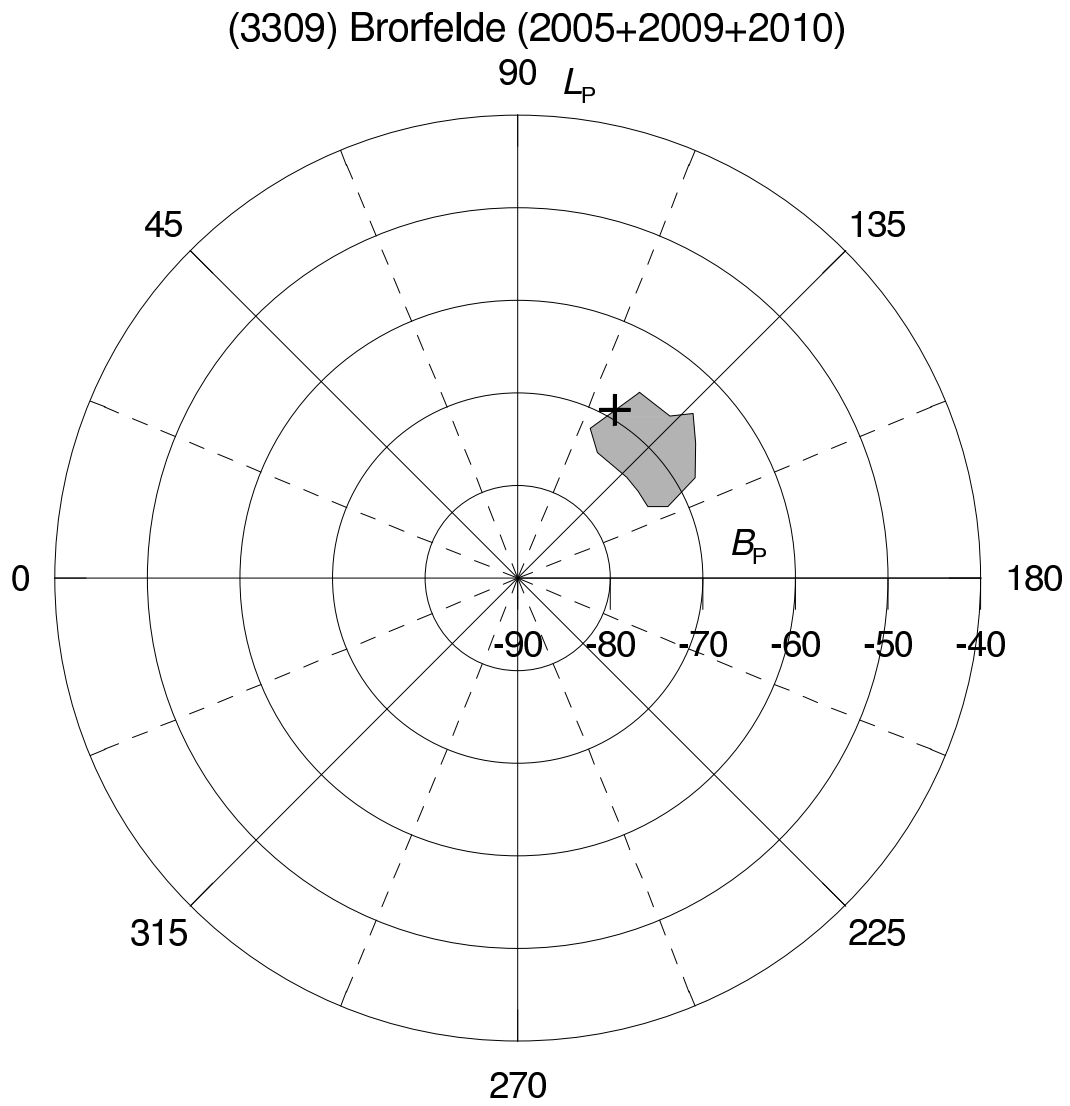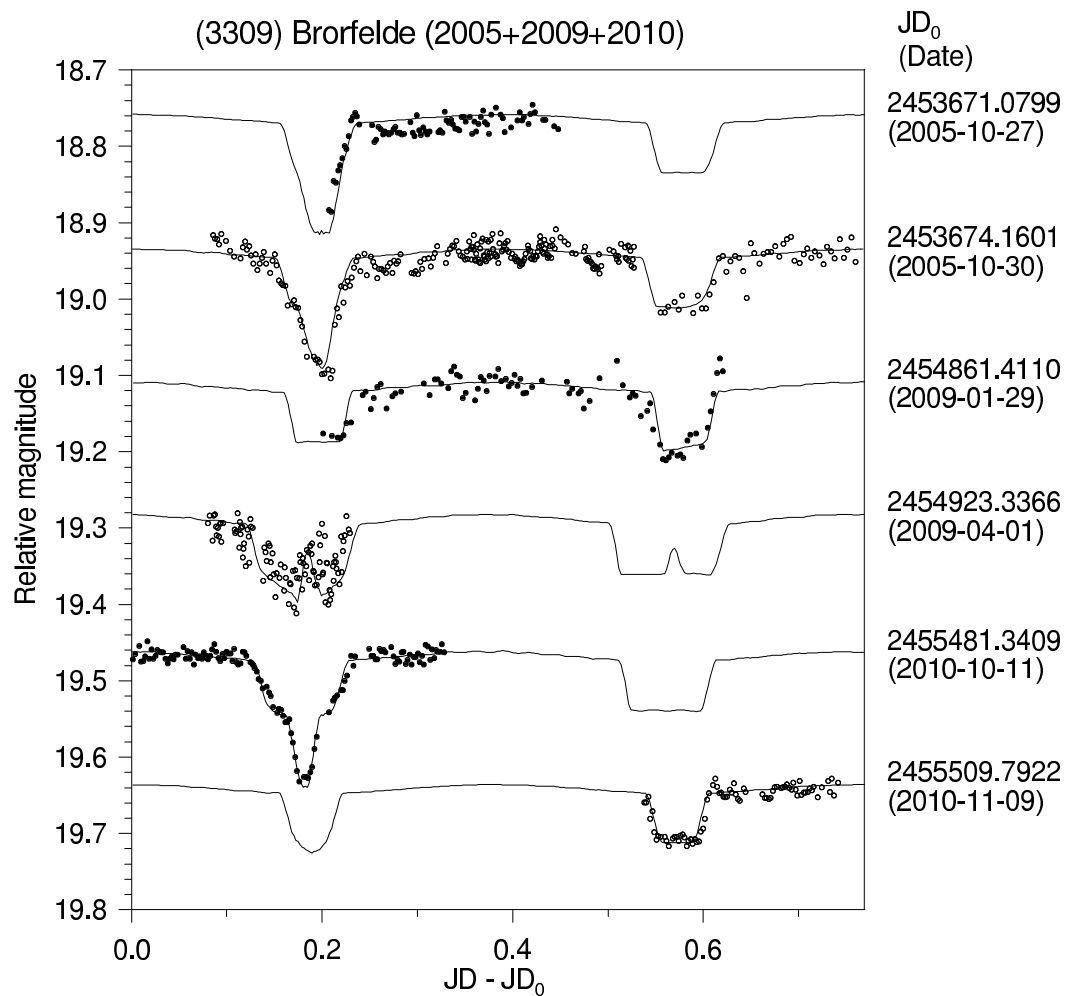
Fig. 5. Same as Fig. 3, but for (1453) Fennia in apparitions 2007, 2009, and 2011. On the fifth curve from the top, the minima are shown in an order opposite (i.e., first the secondary and then the primary event) to the other curves.
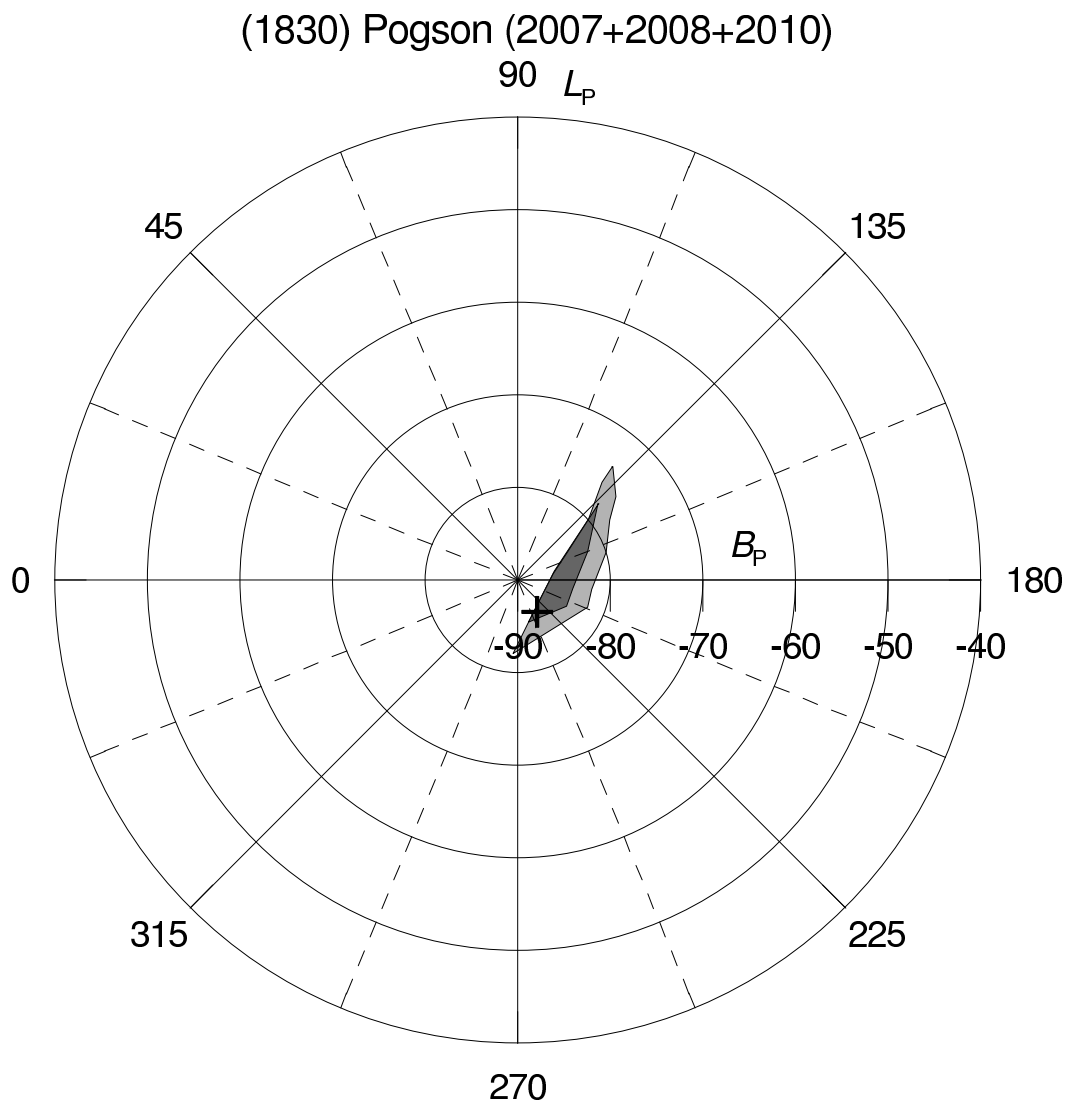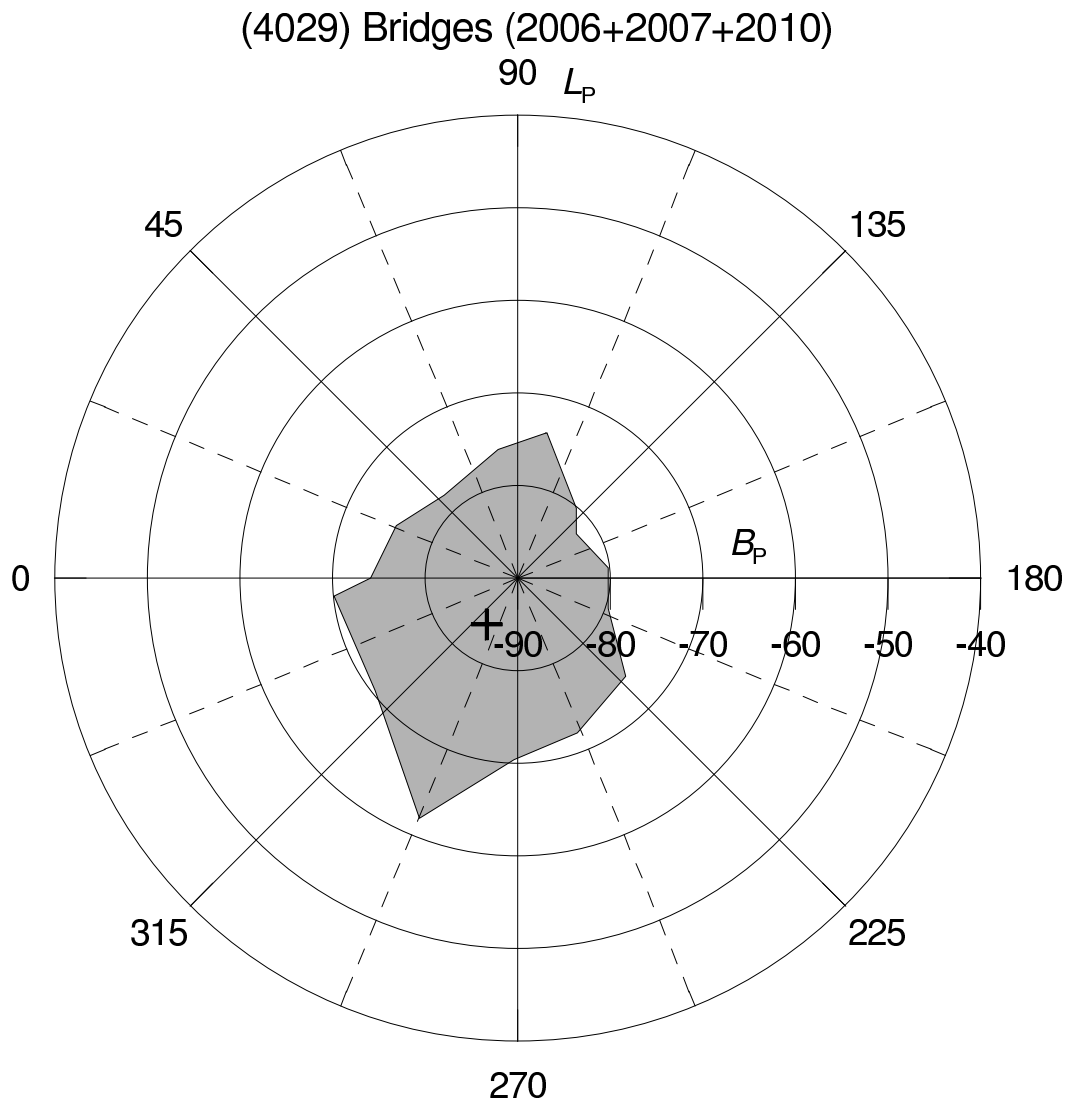
Fig. 6. Area of admissible poles for the mutual orbit of (1830) Pogson in ecliptic coordinates (light gray). To demonstrate the effect of a possible third body on the estimated pole, the dark gray area shows the admissible poles constrained using the effective diameter of the third body set equal to the effective diameter of the primary. The south pole of the current asteroid's heliocentric orbit is marked with the cross.
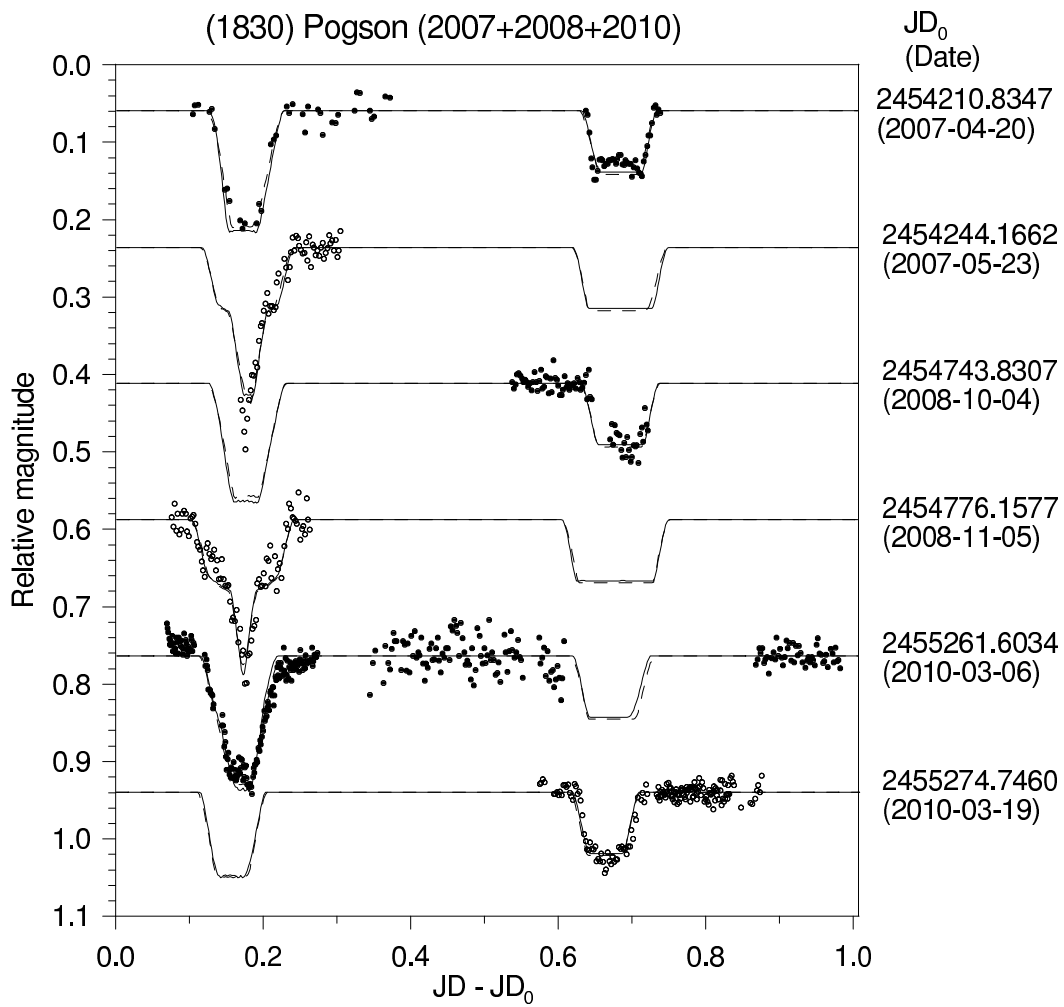
Fig. 7. Same as Fig. 3, but for (1830) Pogson in apparitions 2007, 2008, and 2010. The solid curve denotes the solution assuming a negligible size of the presumed third body, while the dashed curve is the solution with the third body with diameter equal to D_1.
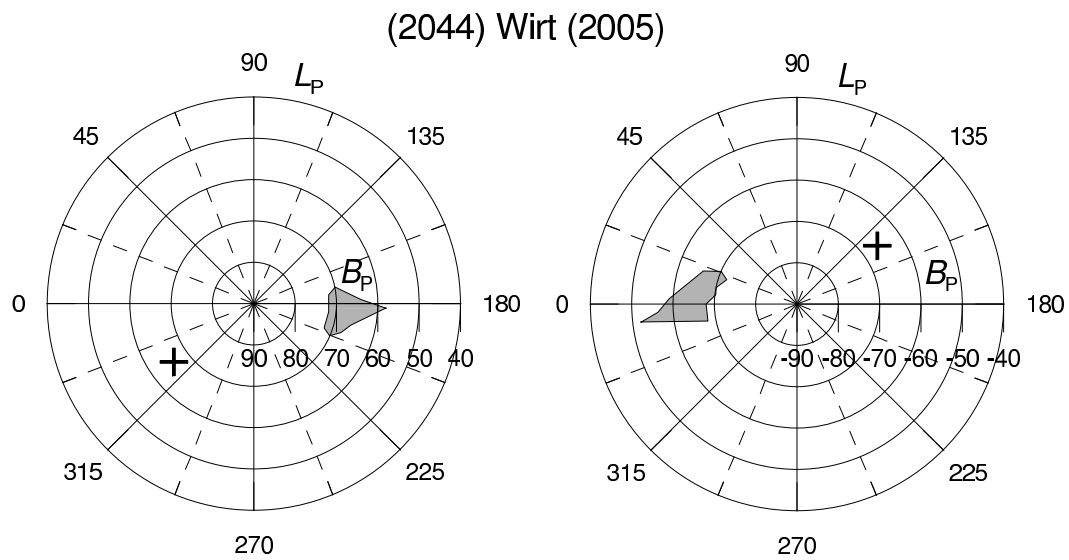
Fig. 8. Area of admissible poles for the mutual orbit of (2044) Wirt in ecliptic coordinates. The north (left) and the south (right) pole of the current asteroid's heliocentric orbit are marked with the crosses.
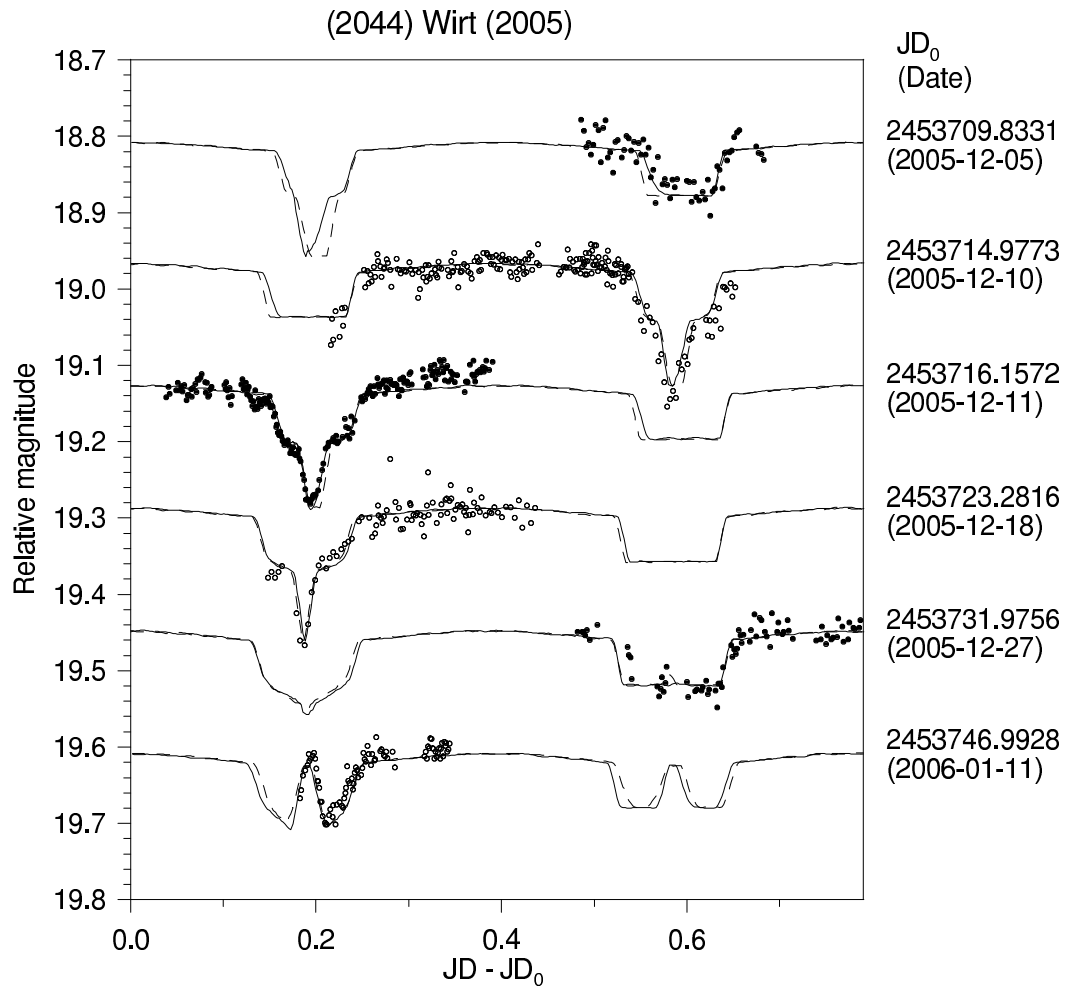
Fig. 9. Same as Fig. 3, but for (2044) Wirt in apparition 2005. The solid and dashed curves denote the retrograde and the prograde solutions, respectively. On the second curve from the top, the minima are shown in an order opposite (i.e., first the secondary and then the primary event) to the other curves.

41
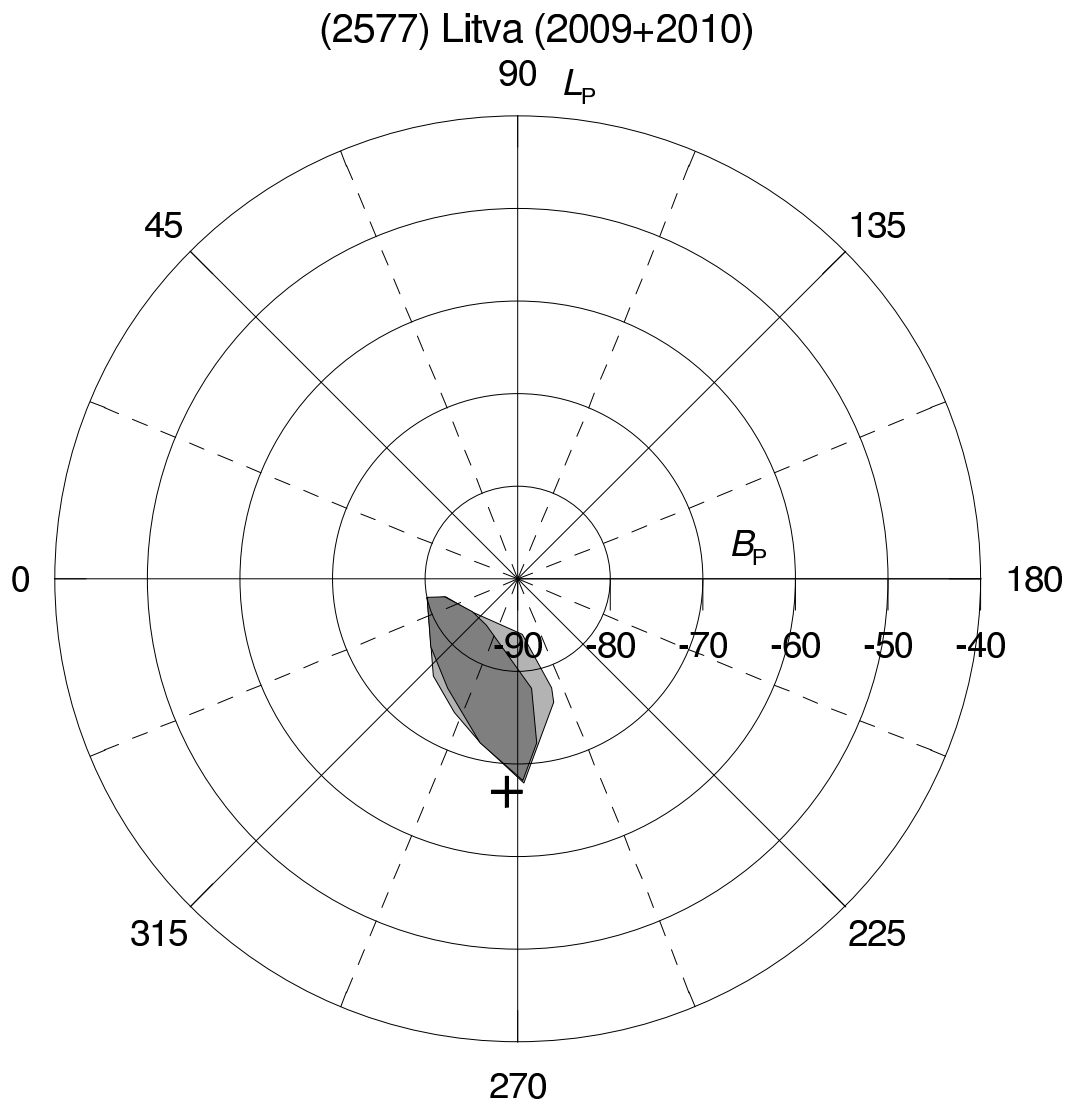
Fig. 10. Area of admissible poles for the mutual orbit of (2577) Litva in ecliptic coordinates (light gray). To demonstrate the effect of a possible third body on the estimated pole, the dark gray area shows the admissible poles constrained using the effective diameter of the third body set equal to the effective diameter of the primary. The south pole of the current asteroid's heliocentric orbit is marked with the cross.
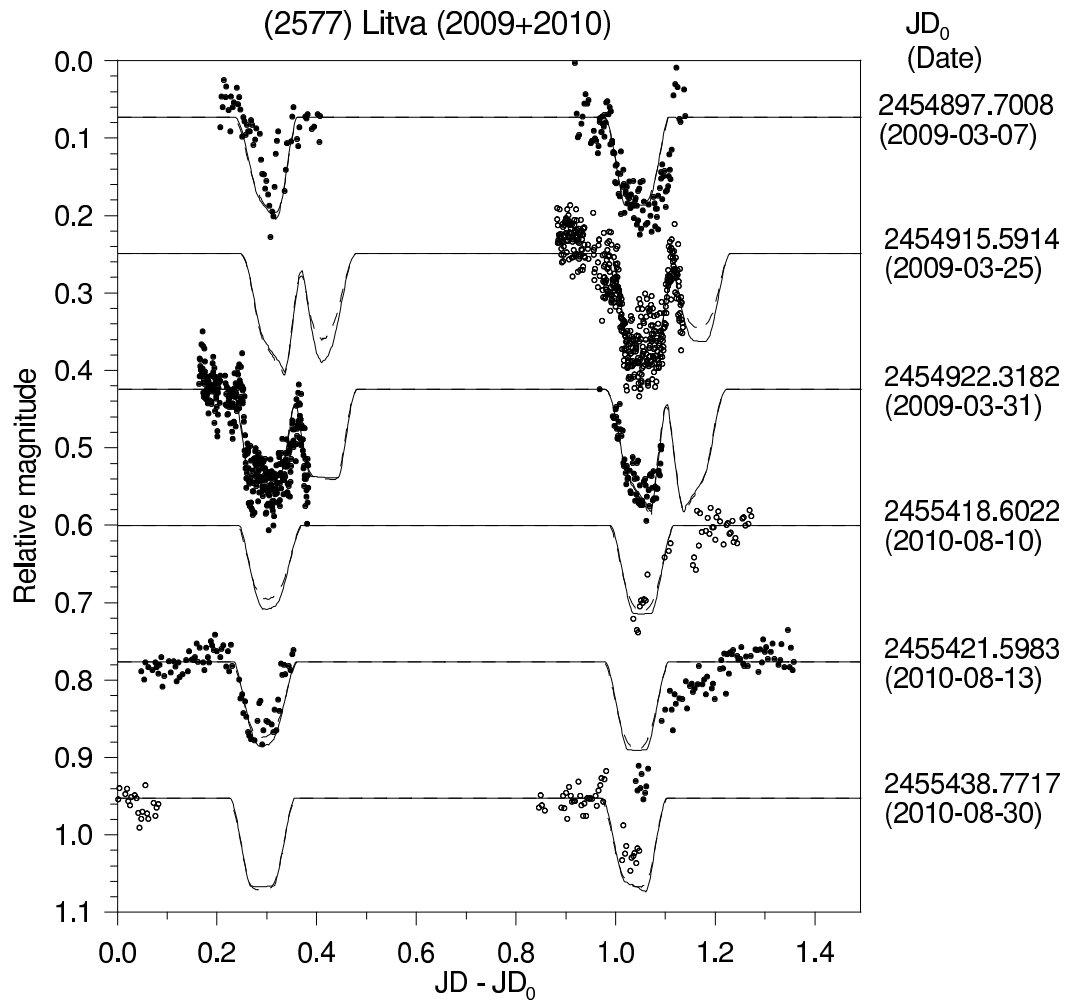
Fig. 11. Same as Fig. 3, but for (2577) Litva in apparitions 2009 and 2010. The solid and the dashed curves denotes the solutions without the third body, and with the third body with diameter equal to D_1, respectively. On the third and the last curves from the top, the minima are shown in an order opposite (i.e., first the secondary and then the primary event) to the other curves.
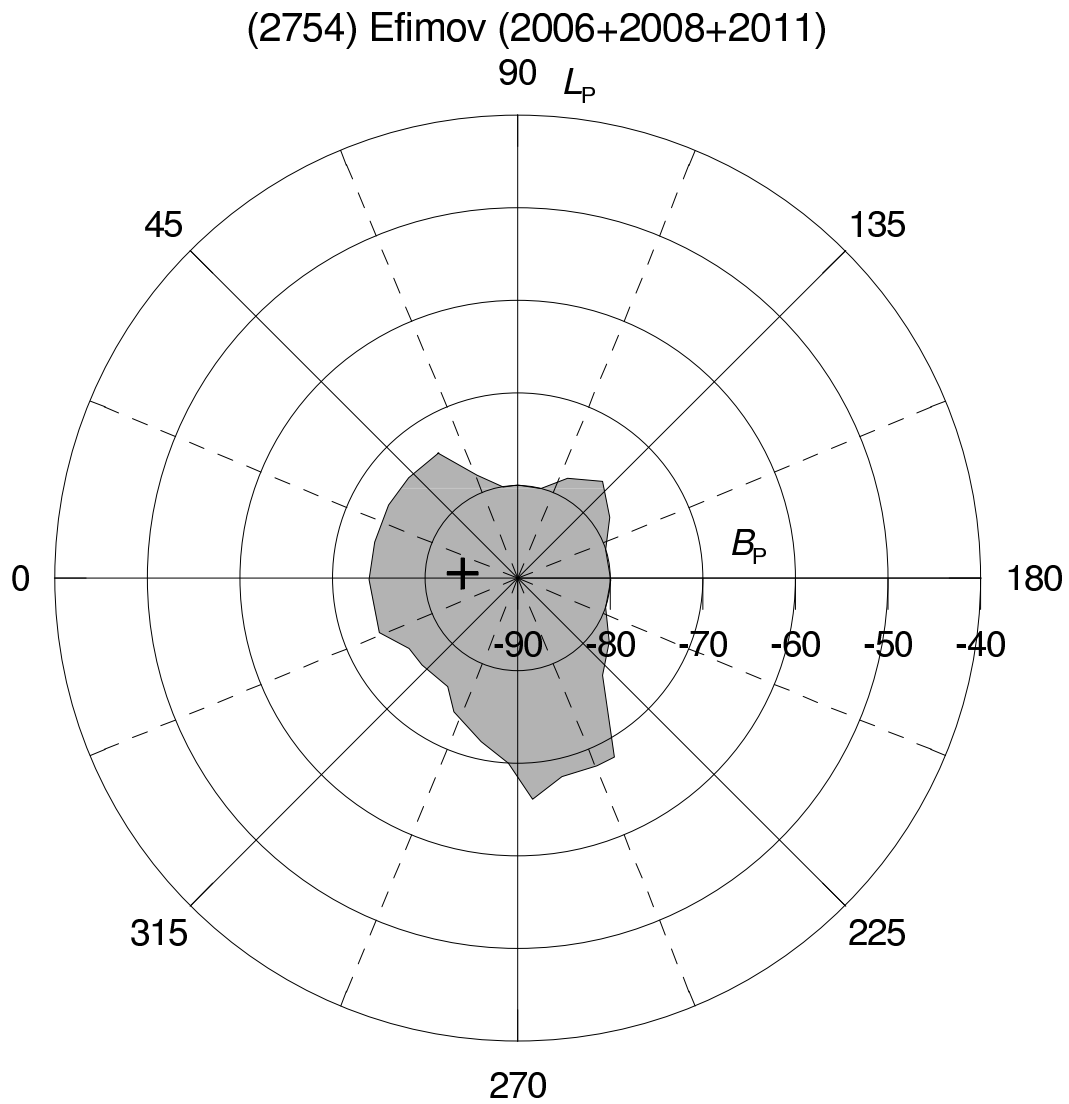
Fig. 12. Area of admissible poles for the mutual orbit of (2754) Efimov in ecliptic coordinates. The south pole of the current asteroid's heliocentric orbit is marked with the cross.

Fig. 13. Same as Fig. 3, but for (2754) Efimov in apparitions 2006, 2008, and 2011.

Fig. 14. Area of admissible poles for the mutual orbit of (3309) Brorfelde in ecliptic coordinates. The south pole of the current asteroid's heliocentric orbit is marked with the cross.

Fig. 15. Same as Fig. 3, but for (3309) Brorfelde in apparitions 2005, 2009, and 2010. On the third curve from the top, the minima are shown in an order opposite (i.e., first the secondary and then the primary event) to the other curves.

47

Fig. 16. Area of admissible poles for the mutual orbit of (4029) Bridges in ecliptic coordinates. The south pole of the current asteroid's heliocentric orbit is marked with the cross.
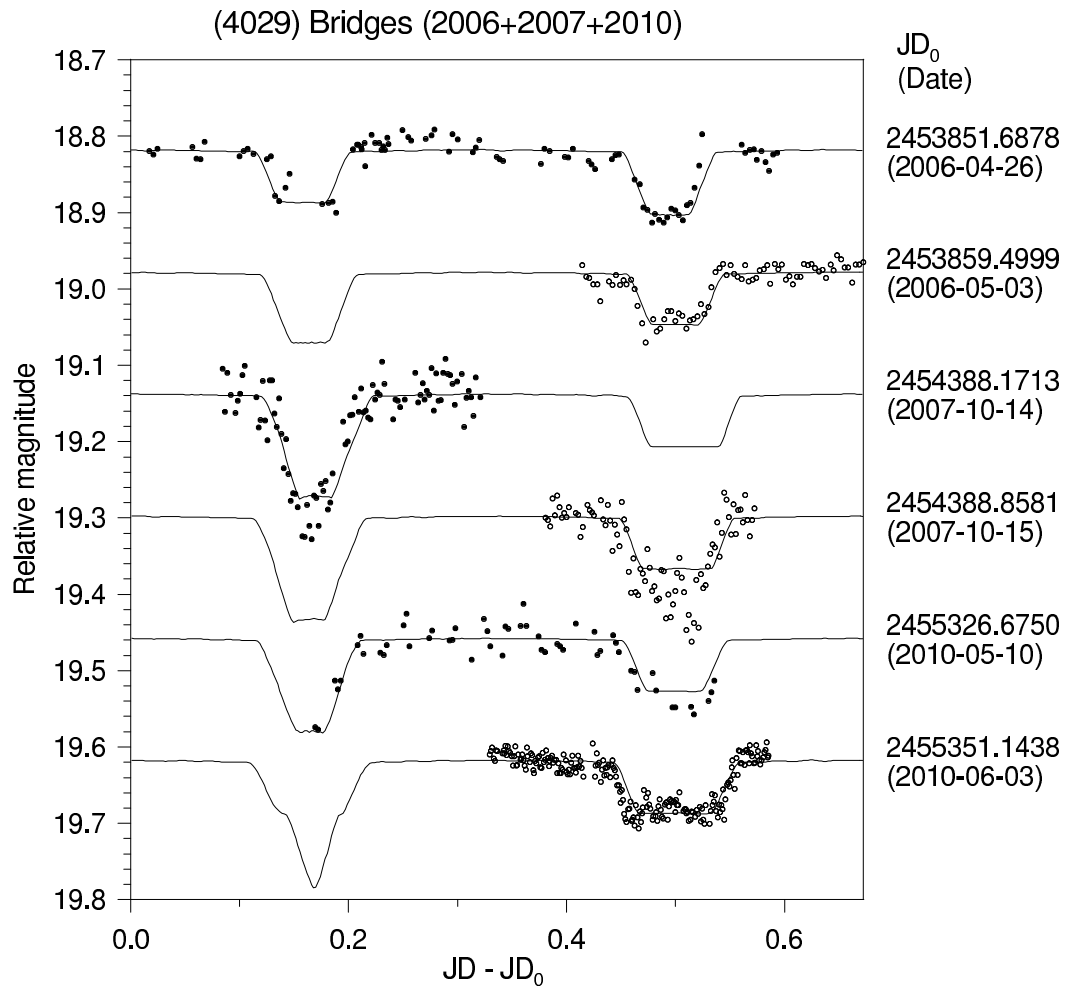
Fig. 17. Same as Fig. 3, but for (4029) Bridges in apparitions 2006, 2007, and 2010. On the first curve from the top, the minima are shown in an order opposite (i.e., first the secondary and then the primary event) to the other curves.
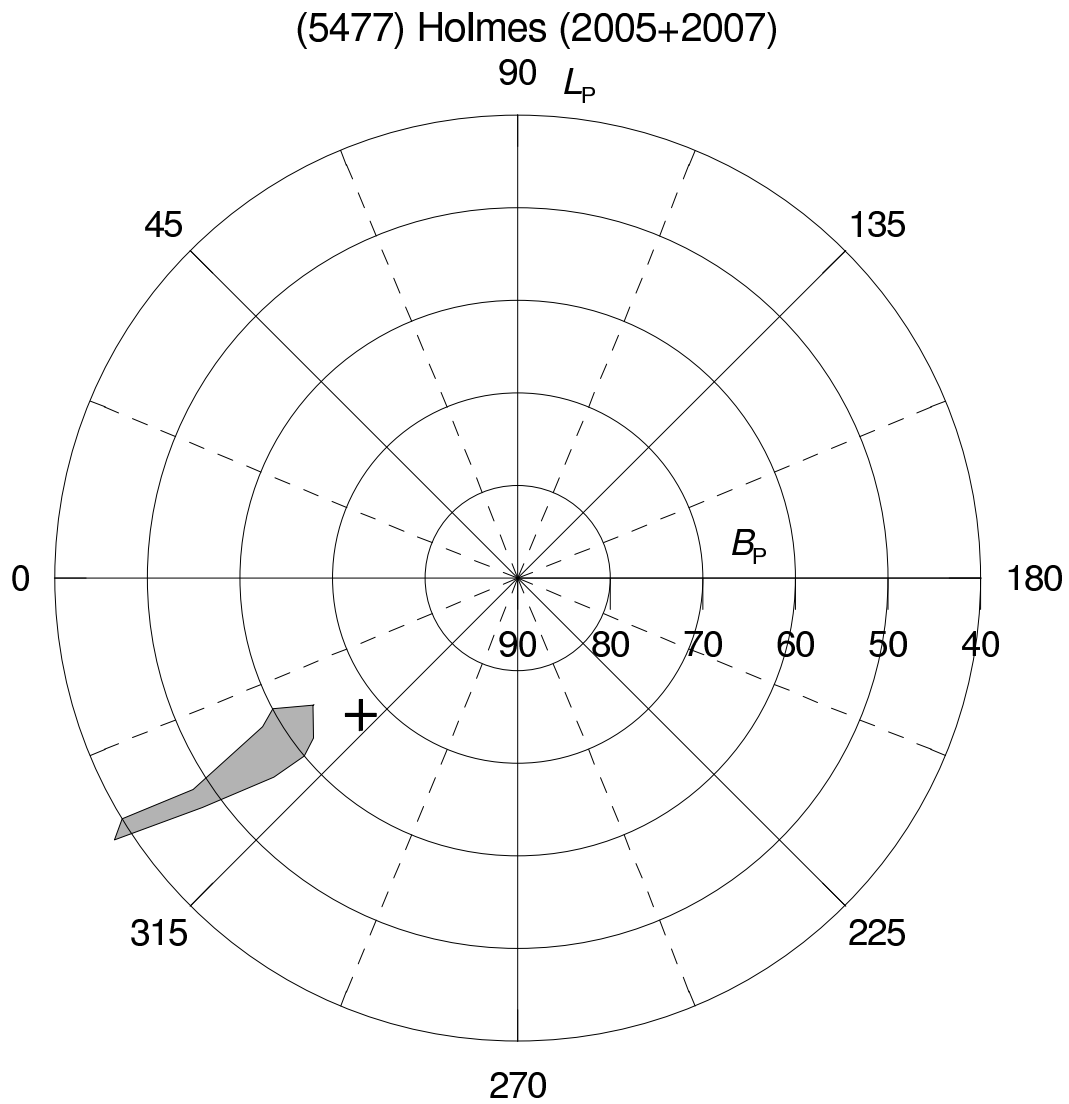
Fig. 18. Area of admissible poles for the mutual orbit of (5477) Holmes in ecliptic coordinates. The north pole of the current asteroid's heliocentric orbit is marked with the cross.

50
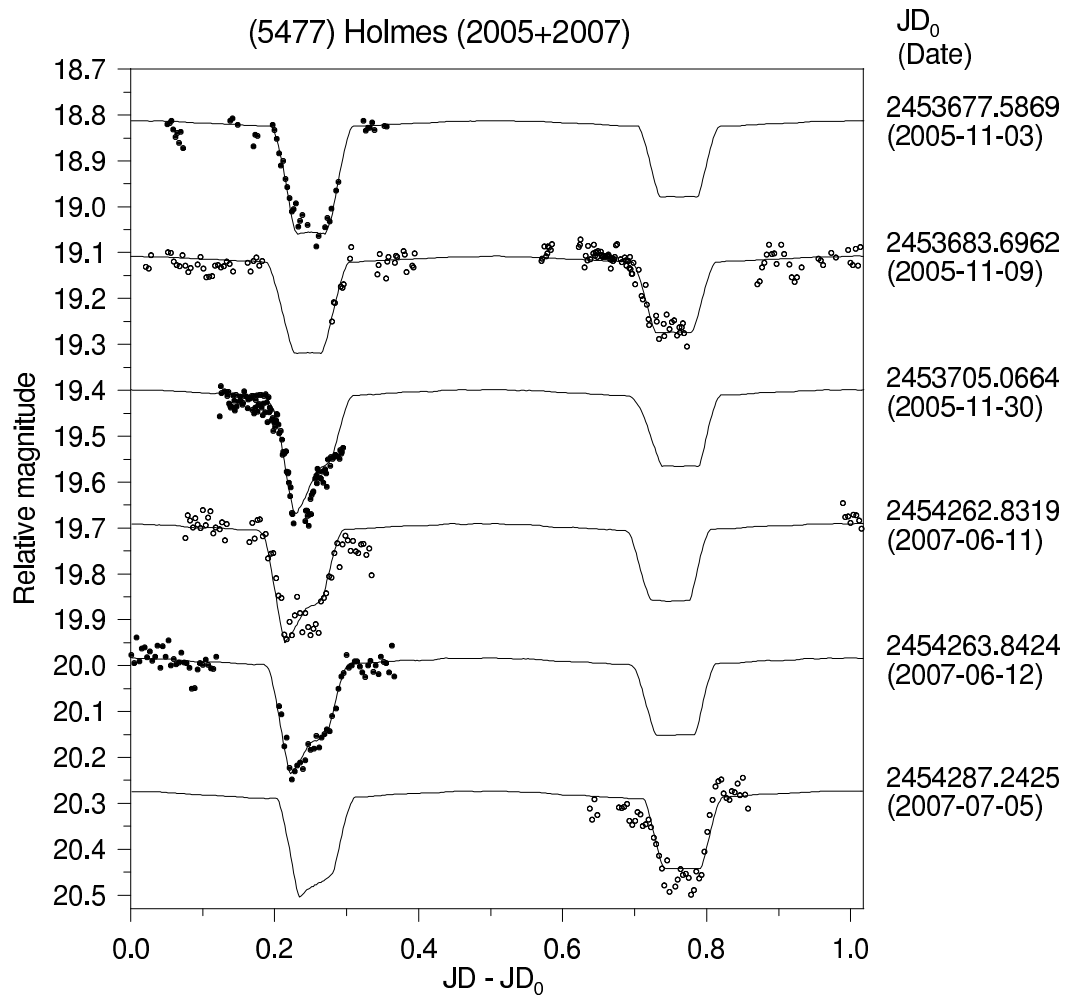
Fig. 19. Same as Fig. 3, but for (5477) Holmes in apparitions 2005 a 2007.
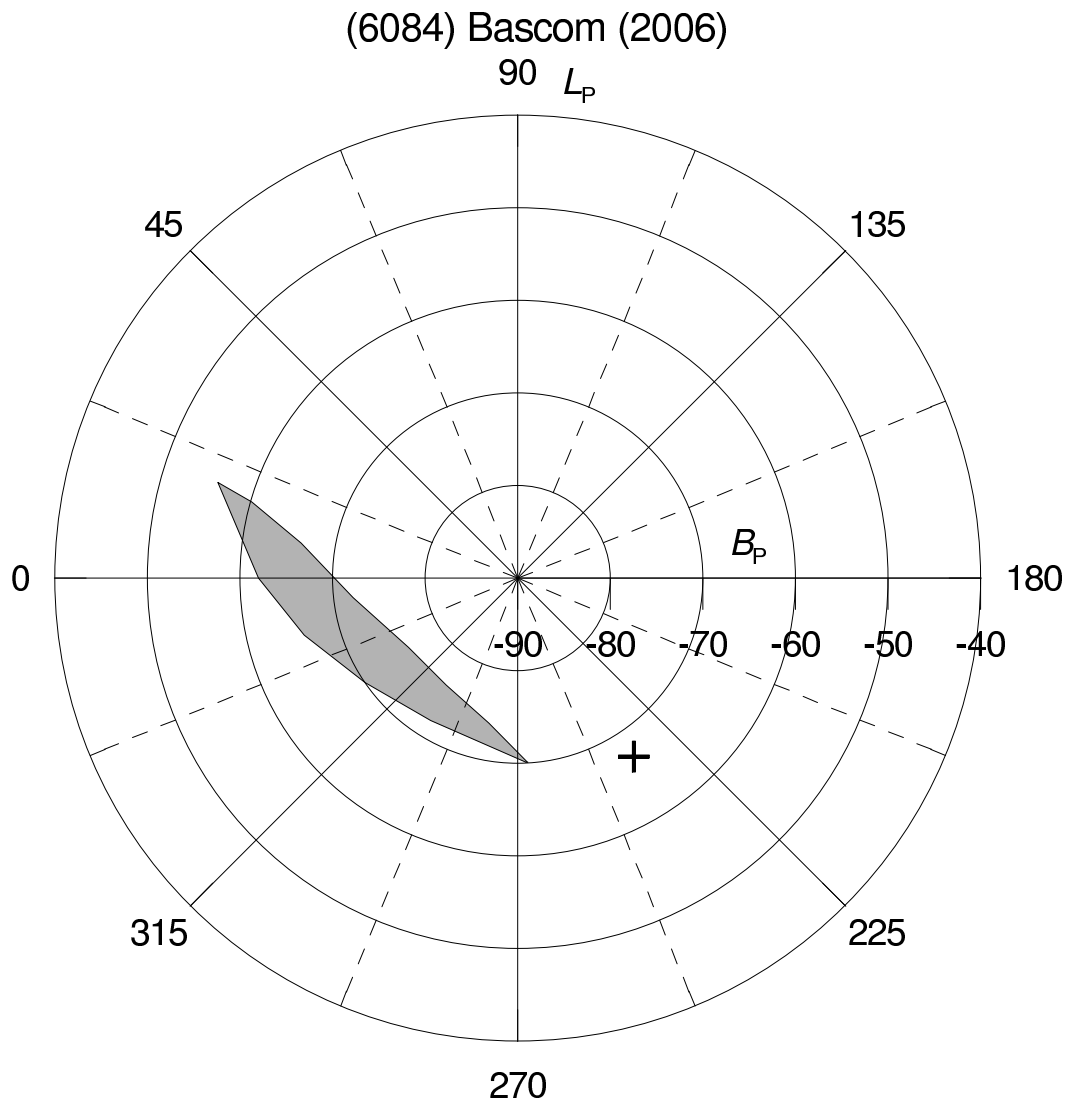
Fig. 20. Area of admissible poles for the mutual orbit of (6084) Bascom in ecliptic coordinates. The south pole of the current asteroid's heliocentric orbit is marked with the cross.
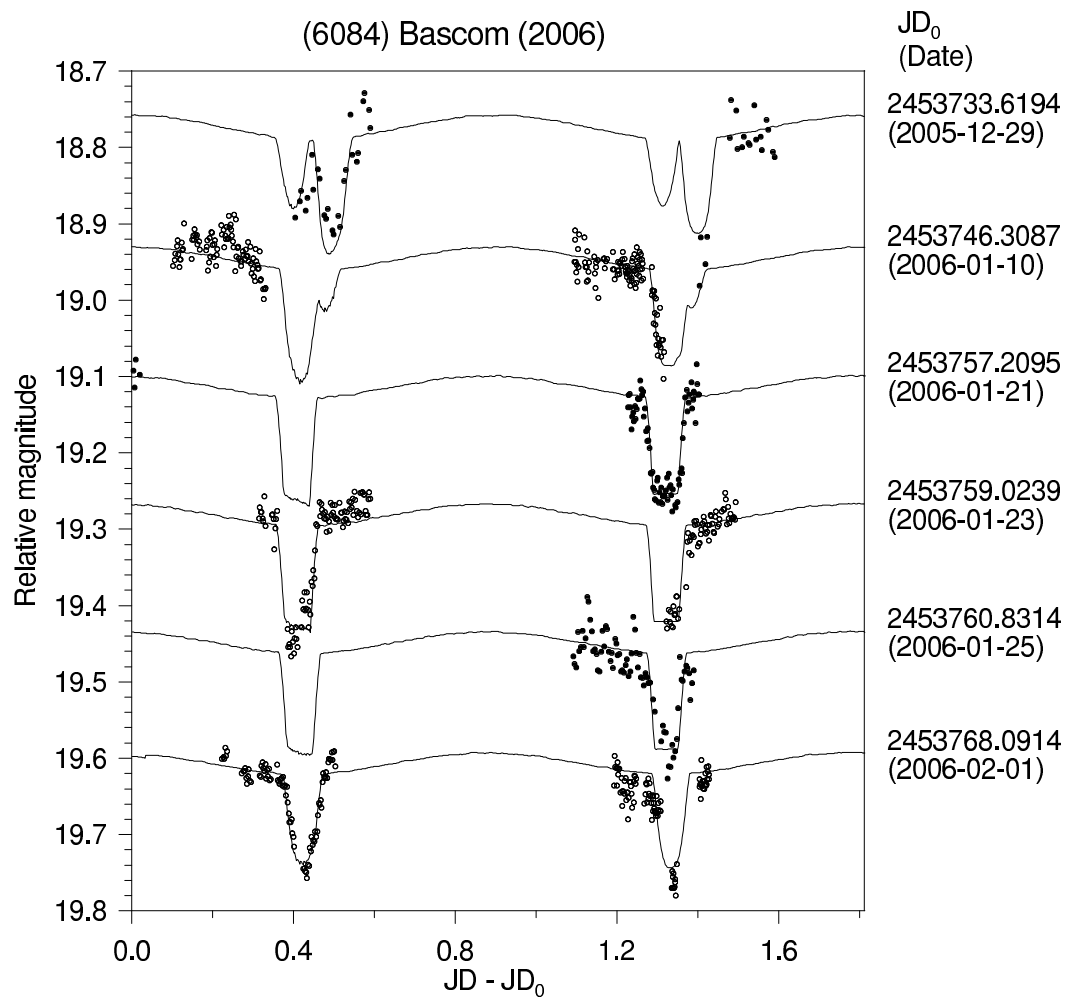
Fig. 21. Same as Fig. 3, but for (6084) Bascom in apparition 2006.
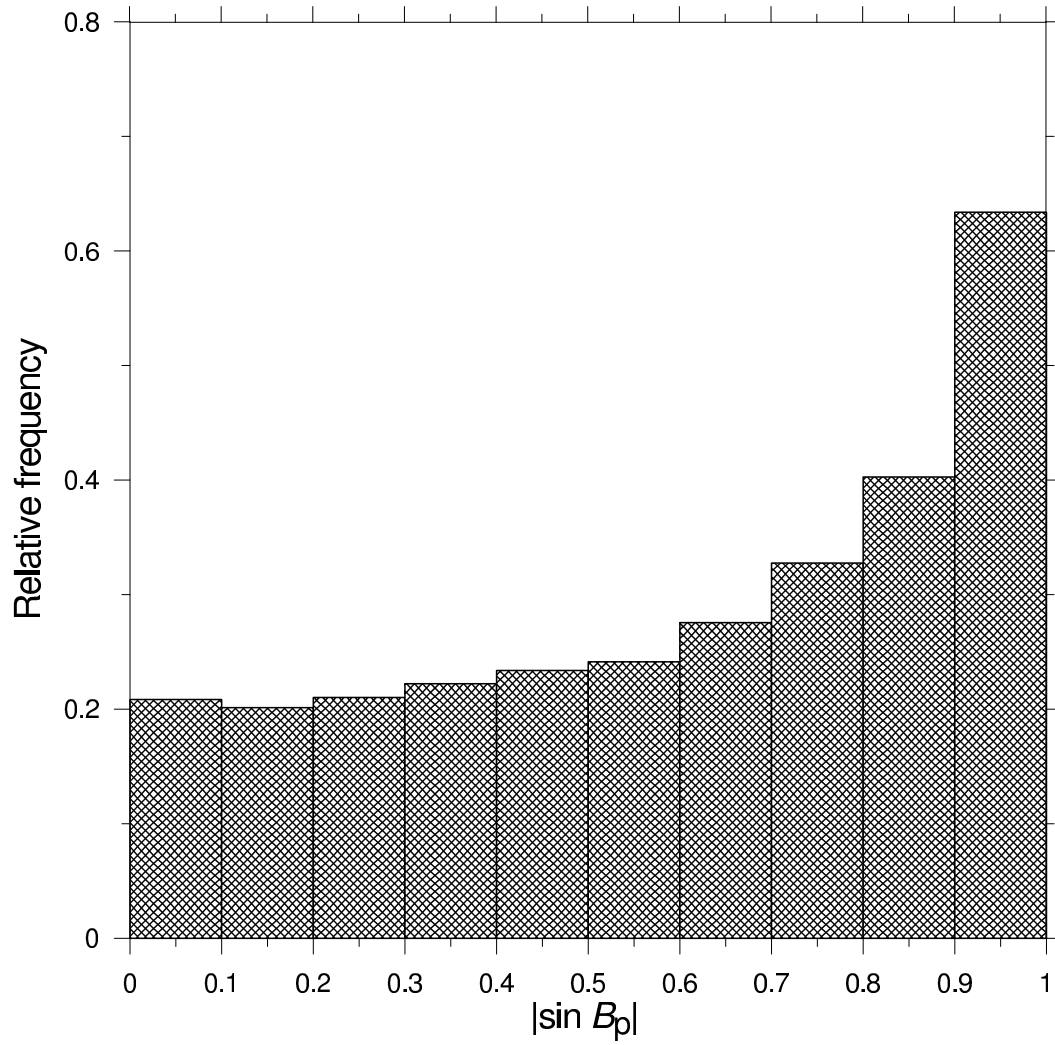
Fig. 22. Relative frequency of the initial positive detections from the survey simulation with the 30000 random pole generations for the 18 binaries for the assumed isotropic distribution of orbit poles vs the sine of pole ecliptic latitude.
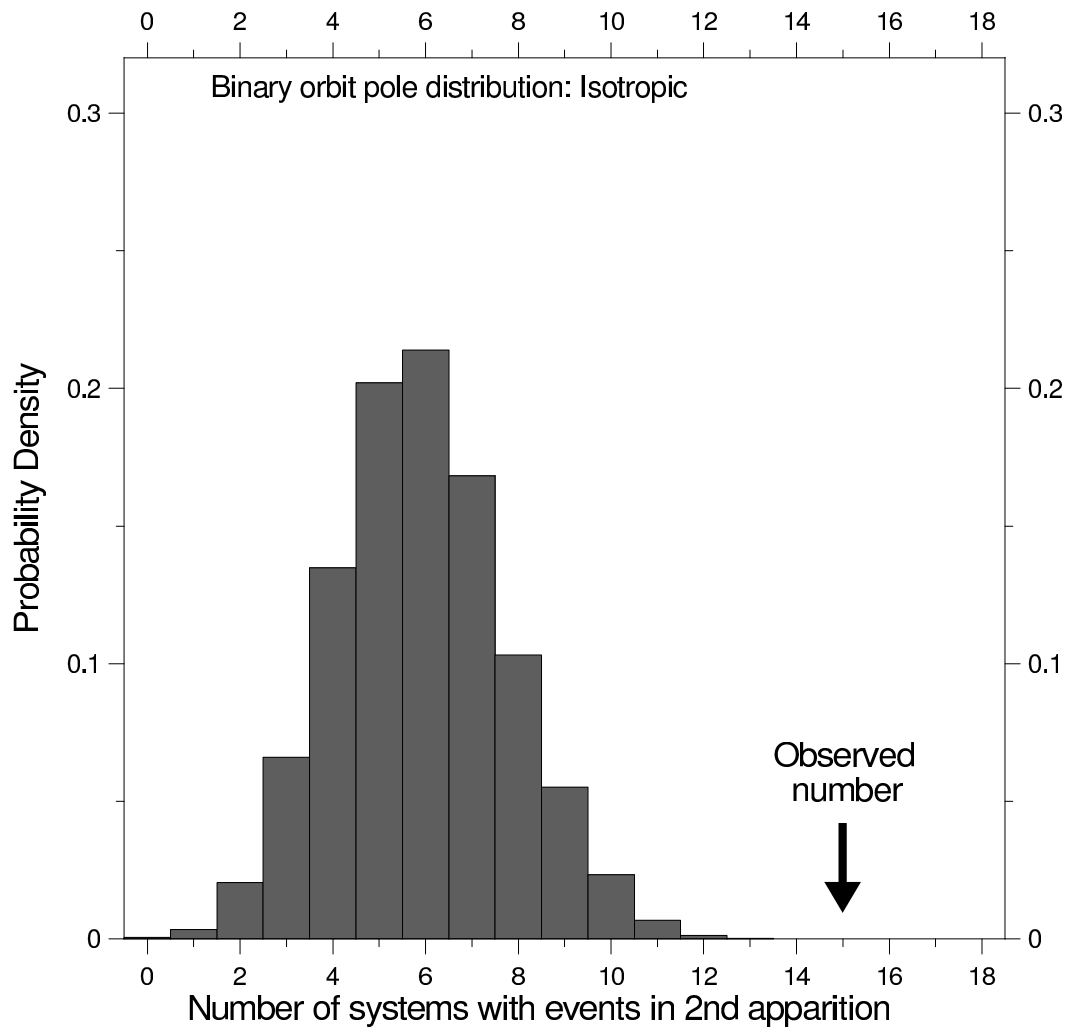
Fig. 23. Estimated probability density of occurrence of mutual events in the return apparition in $N_{2\mathrm{app}}$ of the 18 binary systems, assuming an isotropic distribution of orbit poles of binary systems. The observed number (15) is much greater than the prediction for the null hypothesis.
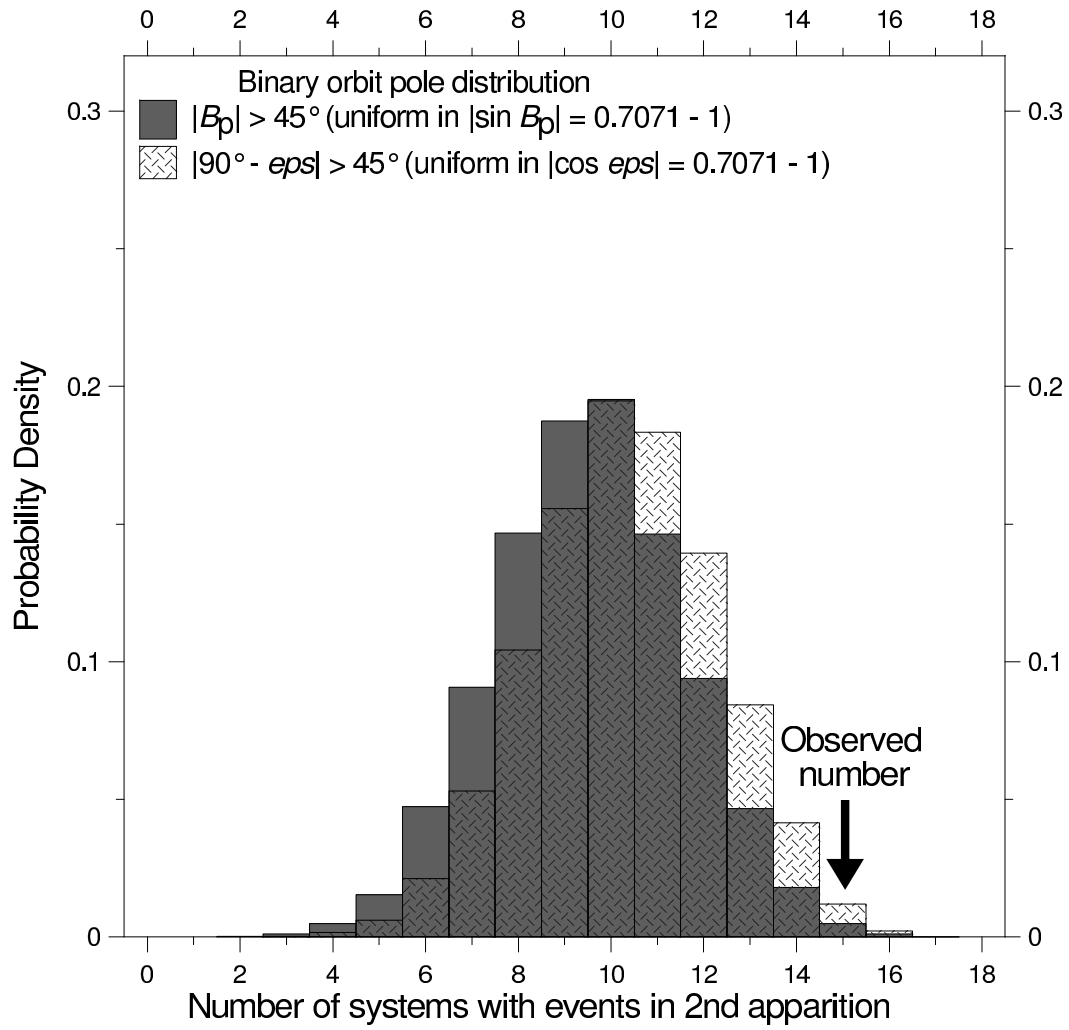
Fig. 24. Estimated probability densities of occurrence of mutual events in the return apparition in $N_{2\mathrm{app}}$ of the 18 binary systems, assuming an uniform distribution of orbit poles of binary systems in $|\sin B_{\mathrm{p}}|$ (filled bins) and $|\cos \epsilon|$ (hatched bins) from $\sin 45°$ to 1.
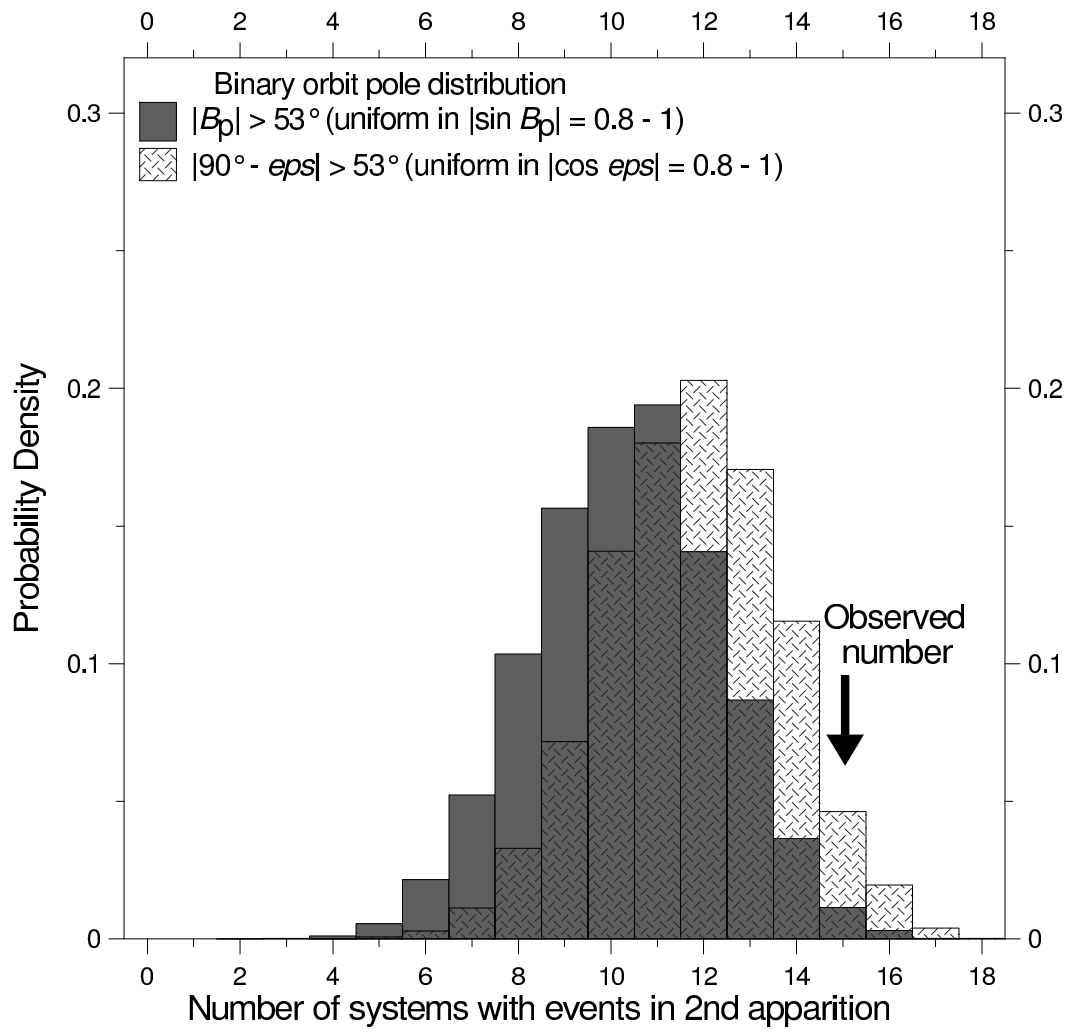
Fig. 25. Same as Fig. 24, but for the cutoff value B_x and $(90° − \epsilon_x) = 53°$.
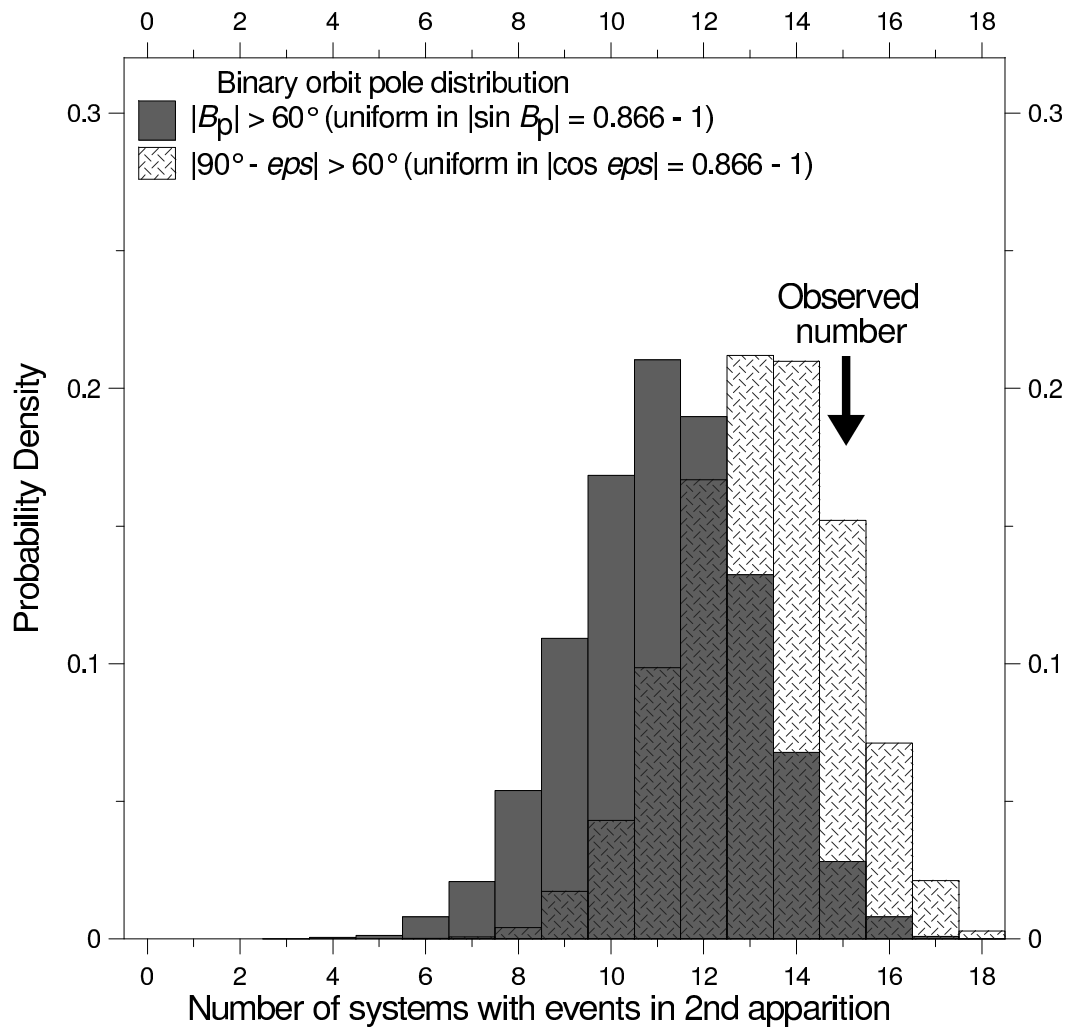
Fig. 26. Same as Fig. 24, but for the cutoff value B_x and $(90° - \epsilon_x) = 60°$.
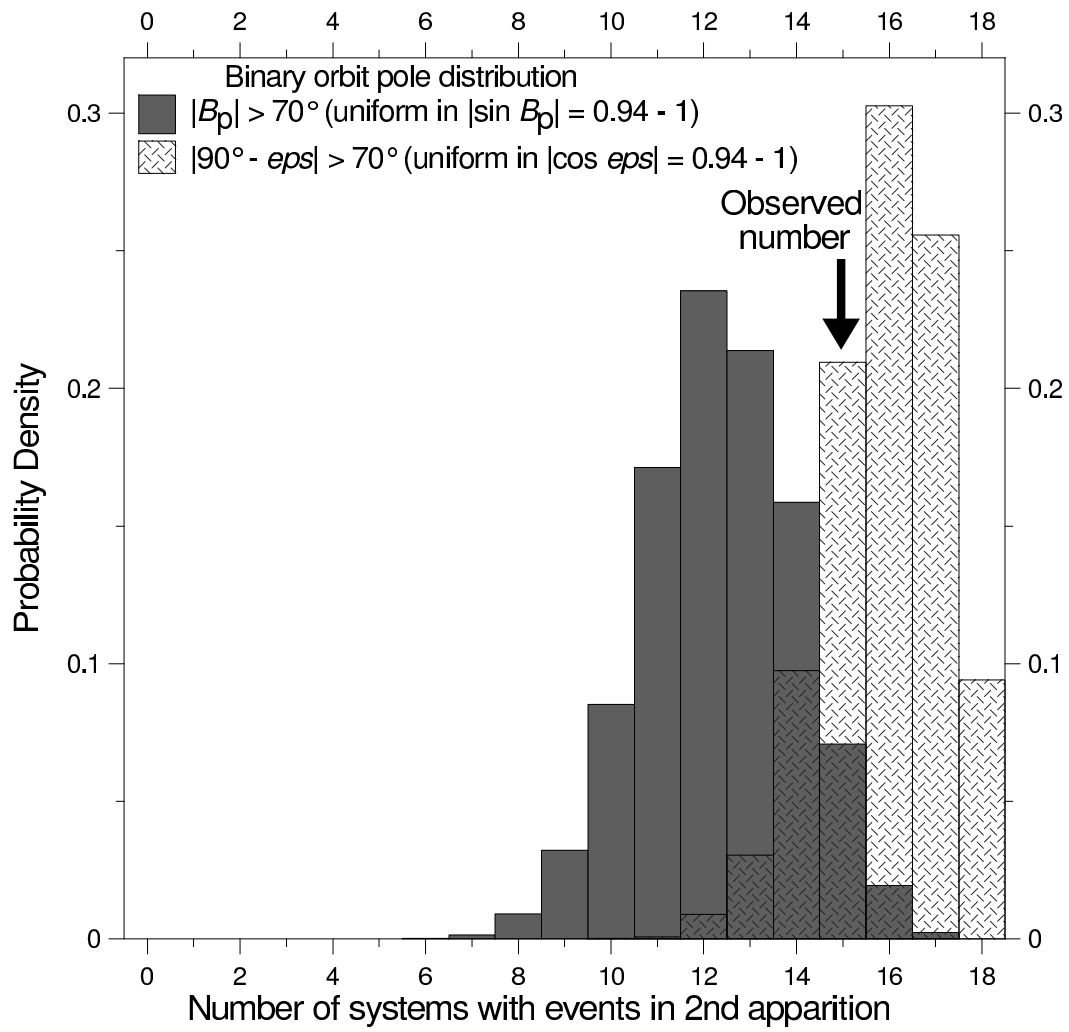
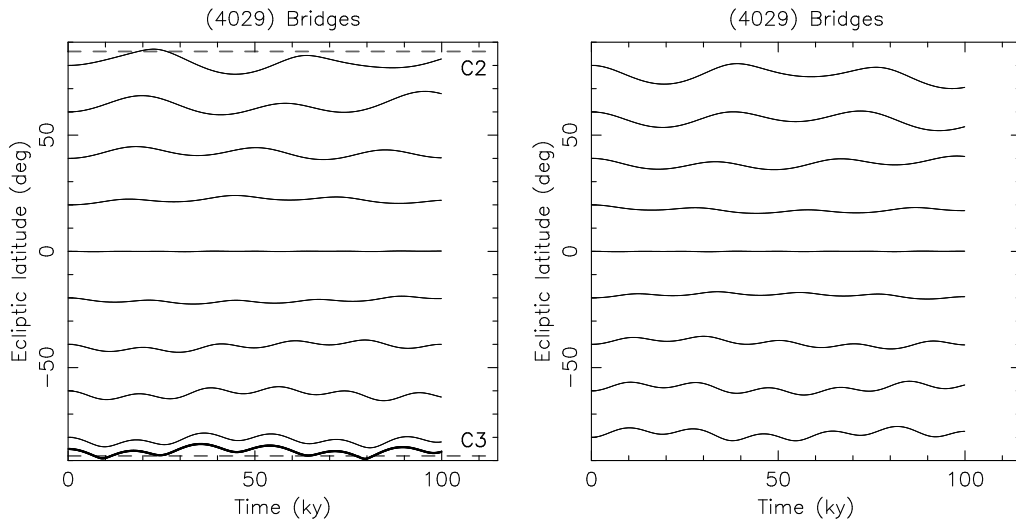Fig. 27. Same as Fig. 24, but for the cutoff value B_x and $(90° - \epsilon_x) = 70°$.

Fig. 28. A sample of evolutionary tracks of the ecliptic latitude (ordinate) of the orbital pole for (4029) Bridges determined by our numerical model; the abscissa is time in ky. Initial ecliptic latitudes B_p were $0°$, $\pm 20°$, $\pm 40°$, $\pm 60°$ and $\pm 80°$. Results on the left panel had initial orbit pole with ecliptic longitude $L_{p,1} = \Omega + 90°$, while those on the right panel had $L_{p,2} = \Omega + 270°$, where Ω is the longitude of ascending node of the binary's heliocentric orbit (cf. Appendix). The gray dashed lines on the left panel show ecliptic latitudes of the Cassini states 2 (C2) and 3 (C3). The thick curve on the left panel shows a possible evolution of Bridges' pole with initial data $(L_p, B_p) = (305°, -85°)$ very close to the osculating pole of the heliocentric orbit and near the center of the uncertainty region of the solution (Table 1 and Fig. 16). All orbits are stable, independently of the latitude value, with only small oscillations due to small value of the heliocentric orbit inclination to the ecliptic.
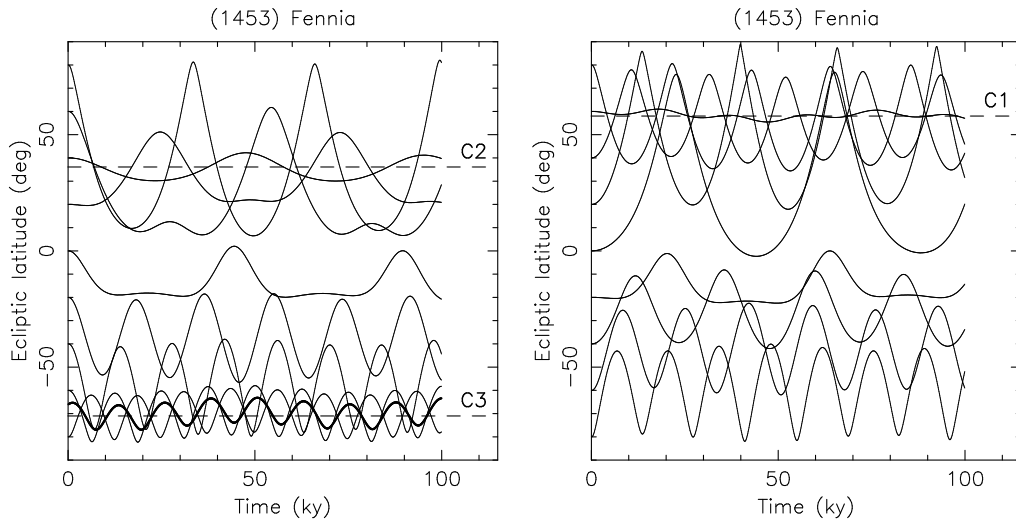
60

Fig. 29. The same as in Fig. 28, but for the Hungaria-class binary (1453) Fennia. The gray dashed lines now show ecliptic latitude of the Cassini states 1 (C1), 2 (C2) and 3 (C3). The thick curve shows a possible evolution of the orbit pole for this binary for initial position $(L_p, B_p) = (95°, -66°)$ very close to the osculating pole of the heliocentric orbit and near the center of the uncertainty region of the solution (Table 1 and Fig. 4).
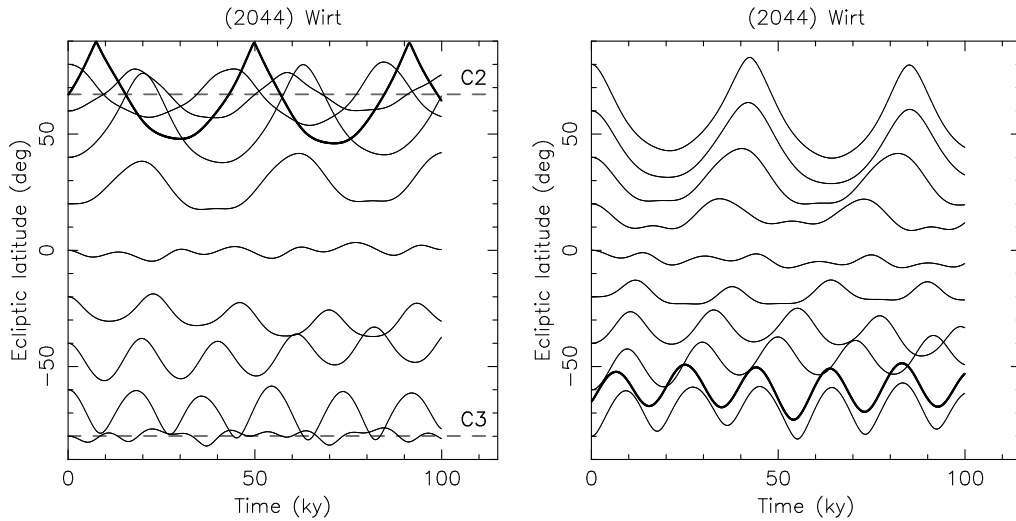

Fig. 30. The same as in Fig. 28, but for the Phocaea-class binary (2044) Wirt. The gray dashed lines now show ecliptic latitude of the Cassini states 2 (C2) and 3 (C3). The thick curves show a possible evolution of the two solutions of the orbit pole for this binary (see Table 1 and Fig. 8): initial pole position $(L_p, B_p) = (180°, 67°)$ on the left panel and $(L_p, B_p) = (0°, -65°)$ on the right panel.